In-Plane Shear Testing of Medium and High Modulus Woven Graphite Fiber Reinforced/Polyimide Composites

M. Gentz, D. Armentrout, P. Rupnowski, L. Kumosa, E. Shin*, J. K Sutter* and M. Kumosa

Center for Advanced Materials and Structures
Department of Engineering, University of Denver
2390 S. York St. Denver, CO 80208

***NASA Glenn Research Center at Lewis Field**
21000 Brookpark Rd.
Cleveland, OH 44135

Abstract

Iosipescu shear tests were performed at room temperature and at 316°C (600°F) on woven composites with either M40J or M60J graphite fibers and PMR-II-50 polyimide resin matrix. The composites were tested as supplied and after thermo-cycling, with the thermo-cycled composites being tested under dry and wet conditions. Acoustic emission (AE) was monitored during the room and high temperature Iosipescu experiments. The shear stresses at the maximum loads and the shear stresses at the significant onset of AE were determined for the composites as a function of temperature and conditioning. The combined effects of thermo-cycling and moisture on the strength and stiffness properties of the composites were evaluated. It was determined that the room and high temperature shear stresses at the maximum loads were unaffected by conditioning. However, at room temperature the significant onset of AE was affected by conditioning; the thermal-conditioned wet specimens showed the highest shear stress at the onset of AE followed by thermal-conditioned and then as received specimens. Also, at high temperature the significant onset of AE occurred in some specimens after the maximum load due to the viscoelastoplastic nature of the matrix material.

1. INTRODUCTION

Considerable efforts have been underway to develop multidisciplinary technologies for affordable propulsion engine components that will enable the system to operate at higher temperatures with reduced cooling while sustaining performance and durability. As part of these efforts, high temperature polymer matrix composites and fabrication technologies are being developed suitable for manifolds, combustion chamber supports and attachments [1]. The usage of such composites should allow the replacement of heavy metal engine components to provide a greater thrust to weight ratio. Graphite/polyimide woven composites are good candidates for these applications. However, one of the limitations of such composites for engine applications is their low strength under shear and biaxial shear dominated loading conditions at room and elevated temperatures [2-7]. Accurate experimental in-plane shear properties are essential for material selection decision and also as design data.

While the T650-35/PMR-15 composites were focused on high strength/medium stiffness applications, the combustion chamber support structure requires much stiffer fibers. The two candidates that have received a considerable amount of attention are M40J/PMR-II-50 and M60J/PMR-II-50 composite systems. The M40J and M60J fibers are graphite fibers with significantly increased longitudinal stiffness properties in comparison with their T650-35 counterparts. The PMR-II-50 matrix is a polyimide resin with improved high temperature performance compared to PMR-15.

This work is a continuation of a series of experimental and numerical studies on the room and high temperature mechanical properties of woven graphite/polyimide composites subjected to in-plane biaxial shear dominated loading conditions [2-7]. Recently, the mechanical behavior of an eight harness satin (8HS) graphite T650-35/PMR-15 composite was investigated by performing the ±45° tensile and Iosipescu tests at room and 316°C temperatures. It was shown that the onset of intralaminar damage and the shear strength of the composite determined at the maximum loads are very strongly

dependent on the type of test. The biaxial tension/shear stress fields in the gage sections of the ±45° specimens resulted in much lower estimates of the critical loads for the initiation of intralaminar damage and the composite strength, in comparison with the Iosipescu test data. It appears that the weakest mode of failure of the composite at room temperature and at 316°C is the combined effect of tension along the warp and fill tows in addition to shear.

It has been recently shown by Benedikt et al. [8-11] and Rupnowski and Kumosa [7] that the T650-35/PMR-15 systems developed large intralaminar and interlaminar residual thermal stresses during the manufacturing cycle that can significantly affect the failure process of these composites, especially if tested under in-plane biaxial shear dominated loads. The stresses are caused by the large difference in the coefficient of thermal expansion (CTEs) of the graphite fibers and the polyimide resins and the large difference between the manufacturing and in-service temperatures (ΔT). However, in spite of the presence of high residual inter- and intralaminar stresses in the 8HS T650-35/PMR-15 composite after manufacturing, internal cracking in the absence of external loads has not been observed. Even when the composite was rapidly cooled by immersion in liquid nitrogen the residual stresses in the composite were not large enough to generate tow cracking without externally applied loads. Such tow micro-cracks were observed in the composites tested using the Iosipescu shear and ±45° tensile tests when subjected to relatively low loads at room and elevated temperatures.

Since the manufacturing temperature of the M40J/PMR-II-50 and M60J/PMR-II-50 composites is higher than that of the T650-35/PMR-15 system and the stiffness properties of the M40J and M60J fibers are higher than those of the T650-35 fibers, the residual thermal stresses in these two composites could be very high and tow micro-cracking during manufacturing could be significant. If present, the micro-cracks could seriously reduce the strength of the composites, especially when tested under in-plane biaxial shear dominated loads. Therefore, the primary objective of this study was to evaluate the in-plane shear strength properties of the composites based on the high stiffness M40J and M60J graphite fibers with the PMR-II-50 resin at room and elevated temperatures (at

316°C) and compare them with the shear strength of the T650-35/PMR-15 composite.

2. MATERIALS TESTED

2.1 Manufacturing

Three different types of graphite/polyimide composite plates were manufactured at the NASA Glenn Research Center (GRC) per the following specifications:

Composite Systems I and II

Fabric: System I - M40J, 6K, 4HS satin weave, fiber areal weight (FAW) of 215 g/m^2, epoxy sizing 1.2 weight percent. (TORAYCA M40JB-6K-50B, Untwisted, Type 5 sizing).
System II - M60J, 6K, 4HS satin weave, FAW of 215 g/m^2, epoxy sizing 1.8 weight percent. (TORAYCA M60JB-6K-50B, Untwisted, Type 5 sizing).

Matrix: PMR-II-50 (both systems)

Laminate Architecture: 12 plies, $[0_f/90_f/90_f/0_f/0_f/90_f]_{1s}$ symmetric and balanced, 0 degree is the cloth warp direction.

Panel thickness: M40J - 2.44 mm, M60J - 2.34 mm.

Manufacturing: The panel was vacuum bagged in a press and cured according to the process shown in Figure 1a. The panels were then postcured in air for 16 hours at 371°C then cooled to room temperature in four hours.

Composite System III

Fabric: T650-35-35, 3K 8HS cloth, UC309 size

Matrix: PMR-15

Ply Arrangement: Warp-aligned, ±45°, 16-ply with floating undulations.

Panel thickness: 5.46mm.

Manufacturing: The panel was vacuum bagged in a press and cured according to the

process shown in Figure lb. The panels were then postcured in air for 16 hours at 316°C then cooled to room temperature in two hours.

2.2 Thermo-Mechanical Behavior of Constituents

For comparison, mechanical properties and the linear coefficients of thermal expansion (longitudinal and transverse) of the T650-35, M40J and M60J graphite fibers taken from the available literature, [12] are shown in Table 1.

E_L and E_T are the longitudinal and transverse tensile moduli and CTE_L and CTE_T are the longitudinal and transverse coefficients of thermal expansion. Additionally, for the T650-35 fibers $V_{Lf} = 0.2$ (longitudinal Poisson ratio), $V_{Tf} = 0.4$ (transverse Poisson ratio), $G_{Lf} = 27$ GPa (longitudinal shear modulus), $G_{Tf} = 11$ GPa (transverse shear modulus).

The matrix polymers are viscoelastic materials. Their shear moduli, G, dependant on both time and temperature and their thermal expansion coefficients, α, are non-linear functions of temperature. In the case of PMR-15, the G values were determined from the experimental data presented in Ref. 12 and the coefficients of thermal expansion (α) were measured in this program. The Poisson's ratio of the resin was assumed to be unaffected by time or temperature. Both the G(t,T) and α(T) data were determined from the neat polyimide postcured in air with the postcuring cycle the same as the postcuring cycle of the composite.

Using equations 1 thru 5, [8] the shear modulus G(t,T) and the thermal expansion α(T) of the polyimide can be determined at any given time (ranging from 0 to $10^{6.5}$ seconds) and temperature (ranging from room temperature to 348°C).

$$G_{ref}(t) = 10^{(Exp(0.16(-Log(t+.001)+6.5)^{0.5})+7.5)} \qquad (1)$$

The horizontal shift function, $a_h(T)$, is used in the definition of reduced time $\xi(t)$ where T is in °C:

$$a_h(T) = 10^{(-0.66-0.0243(T-288)-5.57*10^{-5}(T-288)^2-1.12*10^{-7}(T-288)^3)} \quad (2)$$

$$\xi(t) = \int_0^t \frac{dt'}{a_h[T(t')]} \quad (3)$$

$$G(t,T) = G_{ref}(\xi) \quad (4)$$

$$\alpha(T) = 3 \cdot 10^{-12} \cdot (104 + T) \cdot (127160 - 548 \cdot T + T^2) \quad (5)$$

The room temperature shear modulus of the PMR-II-50 was found to be 9% higher than that of the PMR-15. This could indicate that as far as the time independent stiffness is concerned both polymers have very similar properties. Since the viscoelastic properties of PMR-II-50 have not yet been thoroughly investigated, in the modeling part of this study the viscoelastic properties of PMR-II-50 were assumed to be the same as those of PMR-15.

2.3 Composite quality evaluation

Acid digestion tests were performed at NASA GRC to determine void volumes and fiber contents following the accepted ASTM standards: ASTM D2734-70 and ASTM D3171-76, respectively. Two specimens were taken approximately 8.4 mm from the edges of the plates. The acid digestion test results are shown in Table 2. Also, the plates were C-scanned at NASA GRC to evaluate their quality using through-transmission techniques with a Physical Acoustic Corp. Model UPKI-T equipped with a 5MHz transducer.

Dynamic mechanical, thermal mechanical and gravimetric analyses (DMA, TMA and TGA) were performed on TA Instruments Models 2940 and 2950, respectively. DMA was performed at a heating rate of 5°C/min. while TMA and TGA were performed at a

heating rate of 10°C/min. The glass transition temperature (Tg) determined from either DMA or TMA and decomposition temperature (Td) by TGA experiments were calculated by the intersection of lines tangent to the knee of their respective transitions. All Tg and Td values were determined while heating the composites in an air environment. The Tg and Td values for the composite systems are shown in Table 2. Td for the M40J and M60J/PMR-II-50 composites and the neat PMR-II-50 resin was 545±5°C.

2.4 Coefficients of thermal expansion

The coefficients of thermal expansions of the three composite systems were measured using a Netzsch DIL 402C dilatometer with a low temperature furnace. The instantaneous expansion rate at 20°C and 316°C as well as the linear expansion rate from 20°C to 316°C were determined for each composite in-plane, or parallel to the weave, and out-of-plane, or through the thickness. The values are listed in Table 3.

The complete curves of $\Delta L/L$ in percent as a function of temperature from -100°C to 400°C are shown in Figure 2a for the in-plane and in Figure 2b for the out-of-plane T650-35/PMR-15, M40J/PMR-II-50, and M60J/PMR-II-50 composites.

2.5 Preconditioning of composite panels and test specimen preparation

The 8HS T650-35/PMR-15 composite was tested as-supplied. The M40J/PMR-II-50 and M60J/PMR-II-50 composites were tested as-supplied and preconditioned by dry thermo-cycling. Thermo-cycling was carried out on dried panels by heating from room temperature to 316°C in two minutes, held at 316°C for ten seconds and rapidly cooled with air to room temperature. The panels were thermo-cycled two hundred times.

After thermo-cycling the Iosipescu specimens were cut from the plates using a water jet. A 0.76 mm diameter stream of a highly pressurized mixture of water and abrasive was used. The Iosipescu specimens were 90 mm long and 20 mm wide with the thickness as

supplied. After cutting, the as-supplied and thermo-cycled M40J/PMR-II-50 and M60J/PMR-II-50 specimens were dried in a vacuum for 24 hours at 80°C followed by 24 hours at 120°C prior to mechanical testing. Wet thermo-cycled specimens were hydrated in a moist environment prior to testing. After water jet cutting the T650-35/PMR-15 specimens were dried in a vacuum for 24 hours at 120°C prior to testing.

2.6 Optical and SEM observations of the M40J and M60J composites before testing

A cross section of the as-supplied T650-35/PMR-15 from optical microscope observations is shown in Figure 3. No visible traces of damage were found on the cross sections of the composite using both optical and scanning microscopes. Optical and scanning microscope micrographs were also taken of both the M40J/PMR-II-50 and M60J/PMR-II-50 composites in both as-supplied (Figures 4a and 5a) and thermo-conditioned (Figure 4b and 5b) states. It can be seen that both the as-supplied composites (Figure 4a, M40J/PMR-II-50; and Figure 5a, M60J/PMR-II-50) have slightly less damage in the form of tow micro-cracks than do the thermo-conditioned materials (Figure 4b, M40J/PMR-II-50; and Figure 5b, M60J/PMR-II-50). The biggest difference is in the amount of cracking in both materials. The PMR-II-50 composites with the M60J fibers have considerably more tow micro-cracks than the PMR-II-50 composites with the M40J fibers. This is easily seen when comparing Figures 4a and 4b with Figures 5a and 5b. The tow micro-cracks in the M40J fiber system were predominantly distributed in the external plies of the laminates.

SEM images were also taken of the tow micro-cracks in the as-supplied M40J and M60J composites. These can be seen in Figure 6a and 6b. By observing the micro-cracks in both figures it can be seen that the micro-features of the tow cracking in both materials are very similar. In both cases, the resin is pulled away from the fiber/resin interface. A closer investigation of individual fibers leads to the conclusion that the resin is pulled away from that region of the fiber that is facing a large localized concentration of resin (see A in Figures 6a and b). When the propagating crack reaches a region of resin it is

disrupted, and the resin appears to be stretched and not broken and the crack starts again after the resin rich region (see B in Figures 6a and b). This morphology was seen in all the cracks examined in the as-supplied composite specimens.

3. TESTING PROCEDURES

The Iosipescu shear tests were performed on a MTS 809 Tensile Torsion test system. The force transducer used had a maximum tensile or compression capacity of 50 kN with a non-linearity of 0.3% of full scale and a hysteresis of 0.15% of full scale. The force transducer was temperature compensated over a range of 21 to 77°C. The stiffness of the load unit, piston rod, and force transducer was 5.6×10^8, 4.5×10^9, and 8.2×10^9 Nm/m, respectively.

3.1 Room temperature Iosipescu tests

Iosipescu test specimens were displaced at a rate of 1.27 mm/min. until failure. Force, displacement, and strain values were recorded every 0.25 seconds. For modulus testing, Micro-Measurements Division Measurements Group Inc. WK series 0°, 45°, 90° strain gage rosettes were used. At each room temperature condition one specimen received gages installed using Micro-Measurements M-Bond 200 adhesive for dry specimens and M-Bond 300 adhesive for wet specimens following Micro-Measurements instructions. The gages were mounted on the front and back surfaces and the effect of specimen twisting was evaluated.

3.2 Iosipescu shear testing at 316°C

Iosipescu shear testing at 316°C was performed in a MTS 651.10E-04 environmental chamber. The Iosipescu fixture and supports were heated in the chamber at 5.7°C/min. to 316 ±1°C and held for one hour. After the hold, the chamber was opened and the test

specimen was mounted in the Iosipescu fixture. Then, the chamber was closed and the temperature of the gage section on each side of the specimen was monitored. Testing proceeded ten minutes after installation of the specimen into the fixture. The shear modulus was not evaluated at 316°C.

3.3 AE monitoring

Two sensors (D9215) from Physical Acoustic Corp. (PAC) with a temperature range of -200 to 540°C with a strong resonance at approximately 120 kHz and a differential output were coupled to both ends of the Iosipescu specimens. Dunegan Corp. model 1801-100H differential pre-amps were used with a gain of 40 dB and a high pass filter at 100 kHz. A Digital Wave trigger module (FTM4000) provided an additional 27 dB gain with a 100-300 kHz band pass filter on both the trigger and the recorded digital signal. The threshold was set to 50 mV after the 67 dB total gain. A digitization rate of 5 MHz was used for each signal with 2048 total points recorded and a 256-point pre-trigger. The voltage range of the digitized signal was ±1.0 V.

With resonant AE sensors, signals from outside the gage section are harder to eliminate than with wideband sensors. Signals external to the gage section that occurred before loading of the specimens were characterized by low amplitude and short duration. An energy filter with a 25 mV threshold on both channels was used to eliminate this type of signal. In the high temperature tests, because of time limitation on specimen loading, the acoustic coupling to one of the AE sensors was poor compared to the opposite sensor. Since signals from the gage section did not always cause a threshold crossing on both channels, another type of filter was required. The high temperature chamber around the test setup also caused many more unwanted signals. These signals had higher amplitude but with a short duration. A filter with a 25 mV threshold on only one channel was setup with an additional requirement that a threshold crossing occurred 40 μs after the signal trigger.

4. NUMERICAL EVALUATION OF RESIDUAL THERMAL STRESSES

The residual thermal stresses in the 8HS T650-35/PMR-15 system have been evaluated experimentally and numerically by Rupnowski et al. [7] and Benedikt et al. [8-11]. Both the intralaminar [7] and interlaminar [8-11] residual stresses in the composites were determined. The interlaminar residual stresses were computed on the meso- and micro-levels. In order to determine the magnitude of the residual stresses, the viscoelastic properties of the polyimide matrix must be known. In the analyses performed in Refs. 7-11, the actual viscoelastic properties of the PMR-15 resin were taken. Using the approaches described in [7], the residual thermal meso- and micro- stresses in the M40J and M60J/PMR-II-50 composite system could have also been determined. However, the viscoelastic properties of PMR-II-50 resin are not available at present. Therefore, preliminary computations of the intralaminar residual meso-stresses in the two composite systems were performed using the available elastic properties of the M40J and M60J fibers and their CTEs, and assuming the viscoelastic properties of the PMR-15 resin (instead of the actual PMR-II-50).

Two representative unit cells for the 4HS and 8HS graphite/polyimide woven composites were constructed using finite elements (see Figure 7) and the thermal meso-stresses in the middle of the fill tow were calculated using the procedure developed in Ref. 7. Plane stress conditions were assumed. The elastic properties of the T650-35, M40J and M60J fibers were taken as presented in Table 1 and 3 assuming the viscoelastic properties of the PMR-15 resin. Since the transverse stiffness properties of the M40J and M60J fibers and their transverse CTEs are also not available, these properties were assumed to be equal to the properties of the T650-35 fibers. The development of the in-plane residual transverse meso-stresses in the direction perpendicular to the fibers during the cooling stage of the postcuring cycle for the three composite systems is shown in Figure 8. In addition, the residual transverse stresses (both in-plane and through the thickness) at

room temperature are presented in Table 4.

The data presented in Table 4 and in Figure 8 indicate that the magnitudes of the residual stresses are not only dependent on ΔT but also on the stiffness properties of the reinforcing graphite fibers. Since the cooling rate in the post-curing cycle for the T650-35 system was much faster than for the other two composites, the residual stresses in this composite increase significantly faster than in the other two cases.

It was found that the magnitude of the transverse residual stresses (in-plane) in the M40J and M60J/PMR-II-50 composite was significantly higher than that of the T650-35/PMR-15 system. In addition, the effect of the difference in the longitudinal stiffness properties of the fibers for the same ΔT can be seen in Table 4 and Figure 8 (M40J vs. M60J/PMR-II-50). By increasing the longitudinal stiffness of the graphite fibers by 36% (M60J) with respect to the M40J fibers, the transverse in-plane residual stresses in the fill tows of the composite increased by 3 MPa.

The fact that the residual transverse stresses in the fill tows of the M40J and M60J fiber composites are noticeably higher than for the T650-35/PMR-15 system could explain the lack of tow micro-cracking after manufacturing in the T650-35/PMR-15 composite. However, despite large differences in the longitudinal stiffness properties between the M40J and M60J fibers the difference in the transverse stresses in the composites based on these fibers was found to be rather small (3MPa). This was inconsistent with the significant difference in the process induced micro-crack density between M40J and M60J composites (see Figures 4 and 5). The increased micro-crack density could be caused by the difference in the strength of the interfaces in the M40J and M60J composites. The interfacial strength could be higher in the less stiff M40J fiber composite in comparison with the M60J system.

This discrepancy could also be caused by the insufficiency of the finite element model. Most likely, the assumptions of the same transverse properties of the M40J and M60J fibers (both stiffness and CTEs) in the finite element modeling are responsible for the

small difference in the magnitudes of the residual stresses. Since the actual transverse properties of the M40J and M60J fibers are not available, the accuracy of the numerical predictions of the residual stresses in these two composite systems cannot be improved at the present time.

5. IOSIPESCU TEST RESULTS

Typical Iosipescu shear stress vs. displacement curves for T650-35/PMR-15 and M40J-M60J/PMR-II-50 composites tested at room temperature and at 316°C are shown in Figures 9 and 10 respectively. Since the thickness of the T650-35 fiber specimens was very different from the thickness of the M40J and M60J fiber specimens, the curves in Figures 9 and 10 were not presented in a single figure for comparison.

Figures 11a and 11b show stress vs. displacement diagrams of the M40J and M60J composite specimens respectively. These represent typical examples of the stress vs. displacement curves for each composite at room temperature and at 316°C for various preconditioning.

To evaluate the magnitudes of the out-of-plane deformation of the Iosipescu specimens for the medium and high modulus graphite fibers, the shear stress vs. shear strain diagrams from the Iosipescu specimens with the T650-35, M40J and M60J fibers (without conditioning) tested at room temperature were obtained with the strain gages mounted on the front and back faces of the specimens. Six typical stress/strain curves from these tests (two for each system) are shown in Figures 12 a-c. For small strains these examples are very typical.

The room temperature shear stress vs. strain curves for T650-35/PMR-15, M40J/PMR-II-50 and M60J/PMR-II-50 (averaged from the front and back strain gages) are shown in Figure 13 for comparison. From these curves, the shear moduli of the three composites at room temperature were determined. In addition, the shear moduli of the M40J and M60J composites (dry thermo-cycled and with moisture) tested at room temperature were

measured. The room temperature shear moduli from all room temperature Iosipescu tests are listed in Table 5.

Using AE, the critical shear stresses for the initiation of intralaminar damage in the composite Iosipescu specimens were evaluated following the experimental procedures briefly described in section 3.4 of this paper and in recently published work [4,5]. The shear stresses at the significant onset of AE (non-linear increase of AE signal rate with displacement) were taken as a criteria for the initiation of intralaminar damage [4-6]. The shear stresses at the significant onset of AE and at the maximum loads from the T650-35, M40J, and M60J fiber composite Iosipescu specimens tested without preconditioning at room temperature and at 316°C are listed in Table 6.

The shear stresses at the significant onset of intralaminar damage and at the maximum loads from the M40J and M60J fiber Iosipescu specimens tested after preconditioning at room and high temperatures were also determined. These results are shown in Tables 7a and 7b.

At room temperature, the initiation of AE in the T650-35/PMR-15 specimens as well as in the M40J/PMR-II-50 and M60J/PMR-II-50 (with and without preconditioning) specimens always occurred before the maximum load was reached. This effect is clearly shown in Figure 14 for the M40J and M60J composite specimens where the shear stresses at the significant onset of AE are plotted as a percent of the shear stresses at the maximum loads.

In the as–supplied T650-35/PMR-15, M40J/PMR-II-50 and M60J/PMR-II-50 Iosipescu specimens tested at room temperature, the initiation of intralaminar damage occurred at 89.6%, 34.9% and 15.5% of the maximum shear stresses (see Table 8). For the M40J and M60J fiber systems tested at 316°C, the initiation of AE in several specimens occurred after the maximum load was achieved. This very unusual behavior was marked in Table 6 and Table 7a. The number of asterisks in these tables indicates the number of specimens (out of three for each system) when this mechanism was detected. The onset of AE after

the maximum shear stresses was not observed in the case of the T650-35/PMR-15 Iosipescu specimens and the shear stresses at the onset of AE occurred at 83% of the maximum shear stress.

The failure of the M60J/PMR-II-50 specimens that were thermo-cycled and wet conditioned resulted in the total separation of the two halves of the specimen (failure along the notch root axis). However, this was not observed in the case of the M40J specimens despite the fact that these specimens were tested to larger displacements. Obviously, this is caused by the lower tensile strength and strain to failure of the M60J fibers compared to the strength and strain to failure of the M40J fibers.

In two cases, significant out-of plane deformation of the M40J fiber Iosipescu specimens (one with and one without preconditioning) were observed at 316°C without any noticeable twisting of the M60J fiber specimens tested at this temperature. In addition, crushing of the composites near the inner loading blocks was also detected. All three thermo-cycled/wet M40J fiber specimens, one dry thermo-cycled M60J and two thermo-cycled/wet M60J fiber specimens developed significant crush zones underneath the inner loading blocks during the Iosipescu tests performed at 316°C. Specimen twisting and composite crushing was not observed in the case of the T650-35, M40J and M60J fiber Iosipescu specimens tested at room temperature.

6. DISCUSSION

The most important observation from this research is the effect of fiber type on the in-plane shear strength and shear stiffness of the cross-ply woven fiber reinforced composite systems. If we assume that the stiffness and strength properties of the neat PMR-15 and PMR-II-50 resins are similar and that the composite architectures (4HS vs. 8HS) do not have a significant impact on the composite strength in shear, the effect of the graphite fibers on the strength of the composites can be clearly seen in the data presented in Table 6.

At room temperature, the maximum loads (Table 6) decrease with a decrease in the tensile strength and the strain at failure of the fibers (Table 1). Since the tensile strength and the strain at failure of the M60J fibers is the lowest, the shear strength of the M60J/PMR-II-50 composite is also the lowest. Most importantly, the reduction in the shear strength of the composites at room and elevated temperatures is linearly related to a decrease in the tensile strain at failure of the fibers (see Figure 15). However, the matrix also influences the shear strength of the composites since the elevated temperature strength data are reduced in comparison with the room temperature ultimate shear strengths of the composites. Since the effect of elevated temperatures (up to 316°C) on the T650-35, M40J and M60J fibers should be minimal, the reduction in the composite shear strengths at high temperature must be attributed to the reduction in stiffness and strength properties of the PMR-15 and PMR-II-50 resins. Due to the reduced stiffness of the matrix at elevated temperatures [8,13], rotation of the fibers due to in-plane shear at high temperature is easier and the tensile strains in the fibers reach their critical values at failure at significantly lower applied shear stresses than at room temperature.

Temperature and the type of fiber also affect the damage onset stress from AE. The initiation stress at room temperature in the as-supplied composites were the highest in the T650-35 fiber system followed by the M40J fiber composite and finally by the M60J fiber system. However, the decrease in the damage initiation stress cannot be solely attributed to the changes in the fiber strength and their strains at failure. There seems to be a very strong effect of the residual thermal stresses on the initiation of damage, as indicated by AE, in the composites. This effect can be seen in the temperature dependence of the ratios between the shear stresses at the significant initiation of AE and the maximum shear stresses. At room temperature, these ratios for the T650-35, M40J and M60J composites are 89.6%, 34.9% and 15.5%, respectively (see Table 8). For example, for the M60J/PMR-II-50 composite the significant initiation of intralaminar damage (transverse cracks in the fill and warp tows [4,5]) occurs at loads more than six times lower than the maximum loads. However, at 316°C the ratios for the three as-supplied composites systems are similar and are equal to 83.4%, 92.3% and approximately 80% (the last value is questionable due to problems discussed below).

Since the critical loads necessary to initiate cracks in the tows are strongly related to the type of in-plane loading (in this case the same; almost pure in-plane shear generated by the Iosipescu test) and the magnitude of the residual thermal stresses [7], the shear stresses for the initiation of the intralaminar damage in the M60J fiber composite are very low (six times below the maximum loads). This agrees very well with our initial SEM and optical observations of the as-supplied composite specimens. The magnitudes of the residual stresses in the composite are so high that the tow micro-cracks are formed during the cooling cycle without any external loads being applied (see Figure 5a). The magnitudes of the residual stresses in the M40J fiber composite must be significantly lower since the ratio is 35%. This ratio is still very low in comparison with the ratio for the T650-35 fiber composite, but it is much higher than the ratio for the M60J fiber system.

If the ratio between the shear stress for the initiation of intralaminar damage and the ultimate shear strength at room temperature is a measure of the magnitudes of the residual stresses in a composite, these ratios for the three investigated as-supplied composites systems tested at 316°C should be almost constant. This would indicate that the residual stresses at high temperature were significantly relaxed. These stresses should be fully relaxed in the case of the T650-35/PMR-15 system since the manufacturing and testing temperatures were the same ($\Delta T = 0$), and almost entirely relaxed in the case of the other two systems based on the M40J and M60J fibers ($\Delta T = 56°C$). Again, from the data in Tables 6 and 8 these ratios are high and very similar.

The fact that the shear stresses for the initiation of AE in the M60J fiber composite are 9.9 ± 2.5MPa is rather surprising. Since tow micro-cracks were observed in the as-supplied composite before testing, these stresses should be even lower and almost zero since the critical state of stress for the intralaminar cracking in the composite is the state of residual stresses at room temperature (or perhaps at higher temperatures during the cooling stage of the post-curing cycle). Certainly, no shear stress (or any other stress for that matter) should be required to initiate more micro-cracks in the tows after manufacturing. However, the residual meso-stresses in the composite will relax with an

increase in the number of tow micro-cracks [14]. Tow micro-cracking is a form of residual stress relaxation in a woven composite. Therefore, a 10 MPa shear stress was required to increase the magnitudes of the intralaminar stresses in the composite again to reach the critical stress conditions for the initiation of additional tow micro-cracks in the M60J/PMR-II-50 system tested at room temperature.

At room temperature, there is no dramatic effect of the conditioning (dry vs. thermo-cycled vs. thermo-cycled with moisture added) on the ultimate strength (determined from the maximum loads in shear). This can be seen in the data presented in Figure 11a (M40J composite), Figure 11b (M60J composite) and in Table 7b. For the M40J fiber system, the room temperature ultimate shear strength increases slightly with thermo-conditioning whereas the shear strength of the M60J fiber system slightly decreases with conditioning. At 316°C the shear strength of the composites with and without conditioning is lower (again the matrix effect seen also in the as-supplied specimens). For the M60J fiber systems, conditioning did not affect the ultimate shear strength (see Table 7b). The same could be said about the M40J fiber system. However, specimen twisting quite noticeably affects the data obtained on the wet thermo-cycled specimens at 316°C for this composite. Because of twisting the three data points for the wet M40J specimens are the only unreliable ultimate shear strength results from all the tests performed in this study.

Contrary to the insignificant effect of conditioning on the ultimate shear strength of the M40J and M60J fiber composites, the effect of conditioning on the damage onset shear stress is clearly visible especially at room temperature. The shear stresses at the onset of AE at room temperature gradually increase with conditioning (see Figure 14, Table 7a and Table 8). This effect can be observed in the ratios presented in Table 8. At room temperature, for the M40J fiber composite systems the ratios for the as supplied, thermo-cycled and dried and thermo-cycled with moisture added composites are 35%, 43% and 65% whereas the ratios for the M60J fiber system are 15%, 27.3% and 54.2%. This further demonstrates the effect of the residual thermal stresses on the initiation of intralaminar damage in the M40J and M60J fiber composite systems. As expected, thermo-cycling reduced the residual stresses by forming additional micro-cracks in the

warp and fill tows of the two composites [14]. By adding moisture, the residual stresses were further reduced. The reduction in the residual thermal stresses in both systems due to preconditioning had to be overcome by the application of higher shear stresses necessary to initiate transverse cracks in the warp and fill tows of the composites.

At 316°C the onset of AE may occur after the maximum load has been reached. This very unusual effect can be seen in the data presented in Tables 7a and 8 in the case of the dry (with and without thermo-conditioning) M40J composites and the as-supplied M60J system. This could suggest that the damage initiation in the composite does not start from the formation of tow micro-cracks [4,5] due to large residual and applied stress concentrations near the graphite fibers [7] but by fiber fractures occurring very close to the maximum loads. However, the relaxation of residual stresses and their negligible effect on the damage initiation stresses in the as-supplied and pre-conditioned M40J fiber specimens tested at 316°C can be clearly seen in Table 8. The ratios for the composite are very high (close to 100%) and very similar. For the M60J fiber composite the ratios are also high but lower than for the M40J fiber system. The wet M60J Iosipescu specimens tested at 316°C developed significant crush zones near the loading blocks. Therefore, the low ratios between the initiation shear stresses and the ultimate shear stresses could be caused by the formation of compressive damage in the crush zones making these data points questionable.

The next issue that needs to be addressed is the effect of tow cracking on the ultimate shear strength of the composites. This issue is extremely important. It appears that the intralaminar damage in the composites cannot be avoided due to the presence of large residual thermal stresses in the case of the M60J fiber system (numerous tow micro-cracks present before shear testing) and to a certain extent in the case of the M40J fiber composite (few micro-cracks observed before testing in the as-supplied and slightly more in the pre-conditioned specimens). If the presence of tow micro-cracks in the as-supplied M40J and M60J fiber systems have to be accepted, the effect of these micro-cracks on the ultimate shear strength of the composites must be examined. If the data in Tables 6, 7 and 8 and in Figure 15 are evaluated, it appears that the tow micro-cracks do not affect the

ultimate shear strength of the composites and that the reductions in the ultimate shear strengths of the composites at room and elevated temperatures are only caused by the reduction in the fiber strength (in particular the strain at failure of the fibers) and the strength and stiffness properties of the polyimide resins at 316°C. It seems that for the testing conditions considered in this study tow micro-cracks after their formation do not affect the ultimate shear strength of the composite. However, with long term physical and chemical aging the effect of tow cracking on the composite strength might be entirely different and will need to be thoroughly investigated.

The effects of fiber type, resin and preconditioning on the shear stiffness, and in particular, on the shear moduli of the T650-35, M40J, and M60J fiber systems can be seen in the data presented in Figure 13 and in Table 5. Since the shear moduli of 2HS, 4HS and 8HS composites based on the same fibers and resins are essentially identical [15] the effect of different composite architectures (4HS for the M40J and M60J fiber systems and 8HS for the T650-35 fiber composite) can be ignored. Clearly, the shear stress vs. shear strain curves for the M40J and T650-35 fiber systems tested at room temperature are similar (see Figure 13). However, the curve for the M60J fiber system is significantly below the other two curves, especially at high shear loads.

The shear moduli of the three as-supplied and pre-conditioned composites were determined at low loads (at less than 10% of the ultimate shear strength) and the data are shown in Table 5. The results in this table clearly indicate that there is no effect of preconditioning on the shear moduli of the M40J and M60J fiber systems. Moreover, there is no noticeable difference between the moduli of the M40J and M60J fibers and this is most surprising since the shear stiffness of the composite specimens should be strongly dependent on the stiffness of the fibers. However, despite the fact that the M60J fibers are significantly stiffer that the M40J fibers, the M60J fiber composites developed much more tow micro-cracks during manufacturing and preconditioning than the M40J fiber system. Most likely, the expected increased stiffness of the M60J fiber composites due to the stiffer M60J fibers was eliminated due to the micro-cracking. The effect of micro-cracking on the in-plane shear behavior of the composite could only be visible at

higher loads since the shear stress vs. shear strain curve for the M60J fiber system is significantly below the curve for the M40J fiber composite (Figure 13).

If the shear moduli of the M40J and M60J fiber composites (as-supplied and after preconditioning) are compared with the shear modulus of the T650-35/PMR-15 composite, there appears to be a contradiction in the statement relating the shear stiffness of the composites to the stiffness of the fibers. Since the M40J and M60J fibers are much stiffer than the T650-35 fibers, the shear moduli of the M40J/PMR-II-50 and M60J/PMR-II-50 systems should be higher than for the other composite. However, this is not the case if we look at the data presented in Table 5. In the previous work, it has been reported that the shear modulus of the 8HS T650-35/PMR-15 composite at room temperature is somewhere between 5.5 and 6.0 GPa [2-6]. Most likely, the unusually high value of the modulus for the T650-35 fiber composite is a result of the natural variation of stiffness properties of a composite.

Searles et al. [16] recently showed that the out-of plane deformations of woven Iosipescu specimens can be evaluated by monitoring the front and back strains and that the undesirable out-of-plane deformations are caused by the presence of eccentric loads. The largest bending moment, which is responsible for the largest difference in the front to back shear strains, is observed when the eccentric loading conditions simulate the effect of anti-symmetric specimen twisting. This bending moment can be reduced, but not entirely eliminated if long loading blocks are employed in the Iosipescu shear test. The presence of eccentric loads also affects the distribution of shear stresses through the specimen thickness within the gage section. Similar to the effect of eccentric loads on the surface shear strains, their influence on the shear stress gradients has been found to be most substantial when the specimens were subjected to shear in combination with eccentric twisting.

Since the room and elevated temperature tests on the M40J/PMR-II-50 and M60J/PMR-II-50 systems were performed using relatively thin Iosipescu specimens, some of the shear strength and stiffness data could be affected by out-of-plane deformations

(specimen twisting) and composite crushing underneath the inner loading blocks, especially at high temperature. In the tests on the T650-35/PMR-15 system significantly thicker Iosipescu specimens were used 5.46mm vs. approximately 2.4 mm for the M40J/PMR-II-50 and 2.3 mm for the M60J/PMR-II-50. However, if we examine the data presented in Figures 12, the most important observation based on these three figures is the similarity of the curves for each system indicating that the Iosipescu specimens with either T650-35 or M40J and M60J fibers are not prone to undesirable out-of-plane deformations at room temperature. This observation is not surprising regarding the behavior of the T650-35 fiber composite. The fact that the M40J and M60J/PMR-II-50 Iosipescu specimens did not develop any significant out-of plane deformations had to be attributed to the presence of the high modulus graphite fibers. The high stiffness of the M40J and M60J fibers most likely constrained the out-of-plane deformations. Since the out-of-plane deformations of the M40J and M60J specimens were essentially insignificant, the shear stress distributions in the gage section of the specimens were also not affected by twisting. Therefore, the strength data from the dry M40J and M60J/PMR-II-50 specimens are most likely not affected by out-of-plane deformations. Strain gages were not mounted on the 316°C specimens due to a newly discovered negative effect of the presence of high temperature strain gages on the shear moduli and shear strength data of graphite polyimide composites tested at 316°C [6]. Therefore, the lack of twisting could not be confirmed for the high temperature Iosipescu shear tests.

CONCLUSIONS

1. It appears that the ultimate shear strength of woven graphite fiber/polyimide composite is proportional to the strain at failure of the fibers. It was found that the room and high temperature (at 316°C) ultimate shear strengths of the T650-35/PMR-15, M40J/PMR-II-50 and M60J/PMR-II-50 composite systems tested using the Iosipescu shear test increased linearly with an increase in the strain at failure of the T650-35, M40J and M60J fibers. The room and high temperature shear strengths of the M60J fiber system were the lowest followed by the

strengths of the M40J and subsequently T650-35 fiber composite systems. There was no noticeable effect of the thermal conditioning and moisture on the shear strengths of the M40J and M60J fiber composites measured at RT and 316°C.

2. The magnitudes of the residual thermal stresses in the M40J and M60J fiber composites with the PMR-II-50 resin are much higher than in the case of the T650-35/PMR-15 composite. This resulted in the formation of multiple transverse micro-cracks in the fill and warp tows of the composites during manufacturing, particularly in the case of the M60J fiber system. Thermo-cycling and moisture only slightly increased the number of tow micro-cracks in comparison with the as-supplied composites. The exact magnitudes of the intralaminar and intralaminar residual stresses in the M40J and M60J fiber composites cannot be determined at present due to the lack of viscoelastic properties of the PMR-II-50 resin and the absence of the complete set of the physical properties of the fibers.

3. There exists a very noticeable effect of residual thermal stresses on the initiation of intralaminar damage (transverse tow micro-cracks) of the composites subjected to in-plane shear. If the significant onset of AE is taken as an indication and measure of the damage initiation and/or formation, the large magnitudes of the residual stresses in the M60J fiber composite resulted in the formation of the micro-cracks under very low shear stresses at room temperature. At this temperature, the critical shear stresses for the initiation of tow cracking are much higher in the T650-35/PMR-15 and the M40J/PMR-II-50 composites, approximately 90% and 35% of the ultimate shear strength respectively versus 16% of the ultimate shear strength of M60J/PMR-II-50.

4. The critical shear stresses for the initiation of tow cracking in the M40J and M60J fiber Iosipescu specimens increased substantially after preconditioning. This indicates that thermo-cycling (by the formation of addition tow micro-cracks) and moisture can significantly relax the residual thermal stresses in the composites at room temperature. At 316°C the effect of the residual stresses on the initiation of

damage in the as-supplied and pre-conditioned composites appears to be insignificant.

5. Despite the fact that thin M40J and M60J fiber/PMR-II-50 composites plates were tested using the Iosipescu shear test, the obtained room temperature shear strength and shear modulus data are not affected by undesirable out of-plane deformations. This may be attributed to the presence of high modulus fibers in the composites preventing specimen twisting and out-of plane bending.

REFERENCES

1. J.K. Sutter, Higher Operating Temperature Propulsion Components, Proc. of the High Temple Workshop XXII, Edit. DOD/NASA Laboratories and University of Dayton Research Institute, 21-24 January 2002, Santa Fe, New Mexico.

2. K. Searles, G. Odegard, M. Kumosa and M. Castelli, Failure Investigation of Graphite/Polyimide Fabric Composites at Room and Elevated Temperatures using the Biaxial Iosipescu Test, *J. Composite Materials*, Vol. 33, No. 22, pp. 2038-2079, 1999.

3. G. Odegard, K. Searles and M. Kumosa, Nonlinear Analysis of Woven Fabric-Reinforced Graphite/PMR-15 Composites under Shear-Dominated Biaxial Loads. *Mechanics of Composite Materials and Structures*, Vol. 7, pp. 129-152, 2000.

4. G. Odegard, D. Armentrout, K. Searles, L. Kumosa, J.K. Sutter and M. Kumosa, Failure Analysis of ±45° Off-Axis Woven Fabric Composite Specimens, *J. Composites Technology & Research*, Vol. 23, No. 3, pp. 205-224, 2001.

5. M. Kumosa, G. Odegard, D. Armentrout, L. Kumosa, K. Searles and J. K. Sutter, Comparison of the ±45° Off-Axis and Iosipescu Shear Tests for Woven Fabric

Composite Materials, *J. Composites Technology & Research*, Vol. 24, No. 1, pp.3-16, 2002.

6. M. Gentz, D. Armentrout, P. Rupnowski, L. Kumosa, J. K. Sutter and M. Kumosa, Mechanical Behavior of a Woven Graphite/PMR-15 Composite at Room and Elevated Temperatures Determined from the ±45° Tensile and Iosipescu Shear Tests, *Composite Technology & Research*, submitted for publication.

7. P. Rupnowski and M. Kumosa, Meso- and Micro-Stress Analyses in an 8HS Graphite/Polyimide Woven Composite Subjected to Biaxial In-Plane Loads at Room Temperature, *Mechanics of Composite Materials and Structures*, submitted for publication.

8. B. Benedikt, M. Kumosa, P.K. Predecki, L. Kumosa, M.G. Castelli and J. *K.* Sutter, An Analysis of Residual Thermal Stresses in a Unidirectional Graphite/PMR-15 Composite Based on X-ray Diffraction Measurements, *Composite Science and Technology,* vol.61, no.14, p.1977-1994, 2001.

9. B. Benedikt, P. K. Predecki, L. Kumosa, D. Armentrout, J. K. Sutter and M. Kumosa, The Use of X-ray Diffraction Measurements to Determine the Effect of Bending Loads on Internal Stresses in Aluminum Inclusions Embedded in a Unidirectional Graphite Fiber /PMR-15 Composite, *Composites Science and Technology,* vol. 16, pp.1995-2006, 2001.

10. B. Benedikt, P.K. Predecki, L. Kumosa and M. Kumosa, Measurement of Residual Stresses in Polymer Matrix Fiber Reinforced Composites based on X-ray Diffraction, *Advances in X-Ray Analysis*, vol. 45, 2001 conference, in press.

11. B. Benedikt, P. Rupnowski, L. Kumosa, J.K. Sutter, P.K. Predecki and M. Kumosa, Determination of Interlaminar Residual Thermal Stresses in a Woven

8HS graphite/PMR-15 Composite Using X-ray Diffraction Measurements, *Mechanics of Composite Materials and Structures*, in press.

12. J.B. Donnet, *Carbon Fibers,* Third Edition, pp. 312-316, 1998.

13. G. D. Roberts, D. C. Malarik and J. 0. Robaidek, Viscoelastic Properties of Addition-Cured Polyimides Used in High Temperature Polymer Matrix Composites, Composites Design, *Manufacturing, and Applications; Proceedings of the Eight International Conference on Composite Materials*, S. W. Tsai and G. S. Springer, Eds., Society for Advanced Materials and Process Engineering, Covina, CA, pp. 12-H-1 to 12-H-10, 1991.

14. G.A. Owens and S.E. Schofield, Thermal Cycling and Mechanical Property Assessment of Carbon Fiber Fabric Reinforced PMR-15 Polyimide Laminates, *Composites Science and Technology*, Vol. 33, pp. 177-190, 1988.

15. J. Whitcomb and X. Tang, Effective Moduli of Woven Composites, *Journal of Composite Materials*, Vol. 35, No. 23, 2001.

16. K. Searles, G. Odegard and M. Kumosa, The Effect of Eccentric Loads on the Macroscopic Strain and Stress Distributions in Woven Fabric Composite Iosipescu Specimens, *J. Composite Materials*, Vol. 36, No. 5, pp. 571-588, 2002.

ACKNOWLEDGEMENTS

This research was supported by the Air Force Office of Scientific Research and NASA Glenn Research Center under joint grant F49620-00-1-0159. Additional funds were also provided by the National Science Foundation and the University of Denver from a Major Research Instrumentation Program; Instrument Development and Acquisition grant# CMS-9977735.

Figure Captions

Figure 1a: Manufacturing cycle for the 4HS M40J/M60J/PMR-II-50 composite system.

Figure 1b: Manufacturing cycle for the 8HS T650-35/PMR-l5 composite system.

Figure 2a: Thermal expansions in-plane for the T650-35/PMR-15, M40J/PMR-II-50 and M60J/PMR-II-50 composites as a function of temperature.

Figure 2b: Thermal expansions out-of-plane for the T650-35/PMR-15, M40J/PMR-II-50 and M60J/PMR-II-50 composites as a function of temperature.

Figure 3: Optical micrograph of an as-supplied 8HS T650-35/PMR-15 composite.

Figure 4a: Optical micrograph of as-supplied M40J/PMR-II-50.

Figure 4b: Optical micrograph of thermo-conditioned M40J/PMR-II-50.

Figure 5a: Optical micrograph of as-supplied M60J/PMR-II-50.

Figure 5b: Optical micrograph of thermo-conditioned M60J/PMR-II-50.

Figure 6a: SEM micrograph of as-supplied M40J/PMR-II-50.

Figure 6b: SEM micrograph of as-supplied M60J/PRM-II-50.

Figure 7. Two-dimensional finite element representations of the 4HS (a) and 8HS (b) composite architectures.

Figure 8: Residual transverse stresses σ_x in the middle of the fill tows as a function of time in the 8HS T650-35/PMR-15, 4HS M40J/PMR-II-50 and M60J/PMR-II-50

composites. Starting time, t(0), is immediately following the high temperature 16 hour postcure isothermal.

Figure 9: Typical load vs. displacement diagrams for the T650-35/PMR-15 Iosipescu specimens tested at room and 316°C temperatures.

Figure 10: Typical load vs. displacement diagrams for the M40J/PMR-II-50 and M60J/PMR-II-50 Iosipescu specimens (all dry without thermo-cycling) tested at room and 316°C temperatures.

Figure 11a: Typical load vs. displacement curves for the M40J/PMR-II-50 Iosipescu specimens tested at room and at 316°C under dry, thermo-cycled and thermo-cycled with moisture conditions.

Figure 11b: Typical load vs. displacement curves for the M60J/PMR-II-50 Iosipescu specimens tested at room and at 316°C under dry, thermo-cycled and thermo-cycled with moisture conditions.

Figure 12a: Examples of stress strain curves from the front and back strain gages for the T650-35/PMR-15 composites (as supplied) tested at room temperature.

Figure 12b: Examples of stress strain curves from the front and back strain gages for the M40J/PMR-II-50 composites (as supplied) tested at room temperature.

Figure 12c: Examples of stress strain curves from the front and back strain gages for the M60J/PMR-II-50 composites (as supplied) tested at room temperature.

Figure 13: Shear stress vs. shear strain curves for the T650-35/PMR-15, M40J/PMR-II-50 and M60J/PMR-II-50 composites (as supplied) tested at room temperature.

Figure 14: AE initiation stresses (% of the maximum stresses) for all the M40J/PMR-II-

50 and M60J/PMR-II-50 specimens tested at room temperature.

Figure 15: Shear strength of the as supplied T650-35, M40J and M60J fiber composites at room temperature and 316°C as a function of the fiber strain at failure.

TABLES

Table 1. Selected mechanical properties and CTEs of the T650-35, M40J and M60J graphite fibers.

Properties / Fibers	E_L [GPa]	E_T [GPa]	Strength [GPa]	Strain at Failure [%]	CTE_L [10^{-6}/°C]	CTE_T [10^{-6}/°C]
T650-35	241	20	4.55	1.7	-0.5	10
M40J	377	N/A	4.41	1.2	-0.83	N/A
M60J	588	N/A	3.92	0.7	-1.1	N/A

Table 2. Fiber, resin, void contents, Tg and Td for the three composite systems.

Property / Composite	Fiber by volume [%]	Matrix by weight [%]	Void fraction [%]	Tg [°C]	Td [°C]
T650-35/PMR-15	61.38	31.06	1.35	342	473
M40J/PMR-II-50	58.13	35.98	1.80	389	N/A
M60J/PMR-II-50	58.26	34.1	1.32	376	N/A

Table 3. Coefficients of thermal expansion for the three composite systems (in-plane and out-of-plane) and for the PMR-15 and PMR-II-50 polyimide resins.

CTEs / Material	In-plane and (out-of-plane) at 20°C [10^{-6}/°C]	In-plane and (out-of-plane) at 316°C [10^{-6}/°C]	In-plane and (out-of-plane) between 20°C and 316°C [10^{-6}/°C]
Neat PMR-15	40.85	77.40	54.72
Neat PMR-II-50	39.19	70.85	54.18
T650-35/PMR-15	3.92 (42.06)	6.40 (84.48)	4.93 (53.51)
M40J/PMR-II-50	1.00 (32.24)	2.90 (60.52)	1.28 (48.56)
M60J/PMR-II-50	0.20 (37.30)	0.79 (70.89)	-0.13 (55.22)

Table 4. Numerically estimated residual intralaminar meso-stresses in plane and through the thickness in the three composite systems.

Residual Stresses / Composite Systems	σ_x (transverse in-plane) [MPa]	σ_y (transverse through-the-thickness) [MPa]
8HS T650-35 PMR-15	62	20
4HS M40J/PMR-II-50	78	13
4HS M60J/PMR-II-50	81	13

Table 5. Shear moduli of the T650-35/PMR-15, M40J/PMR-II-50 and M60J/PMR-II-50 at room temperature as a function of preconditioning.

Conditioning / Material	Dry [GPa]	Dry and thermo-cycled [GPa]	Thermo-cycled and moisture [GPa]
M40J/PMR-II-50	5.78	5.29	5.75
M60J/PMR-II-50	5.72	5.63	5.67
T650-35/PMR-15	6.97	N/A	N/A

Table 6. Shear stresses at the onset of intralaminar damage (determined by AE) and at the maximum loads from the Iosipescu tests at room and 316°C temperatures performed on the as-supplied T650-35/PMR-15, M40J/PMR-II-50 and M60J/PMR-II-50 composites (dry without thermal cycling).

	At Room Temperature		At 316°C	
Composite System	Shear Stresses at the Significant Onset of AE [MPa]	Shear Stresses at Maximum Loads [MPa]	Shear Stresses at the Significant Onset of AE [MPa]	Shear Stresses at Maximum Loads [MPa]
T650-35/PMR-15	94.8 ± 1.3	105.8 ± 2.6	59.9 ± 1.2	71.8 ± 4.2
M40J/PMR-II-50	30.3 ± 3.1	86.7 ± 2.7	56.5 (one test) (**54.9 ± 4.3)	61.2 ± 4.1
M60J/PMR-II-50	9.9 ± 2.5	63.8 ± 0.4	(*** 40.0 ± 5.8)	50.2 ± 0.8

Number of * are the number of tests with onset of AE after the maximum load.

Table 7a. Shear stresses at the onset of intralaminar damage (determined by AE) from the Iosipescu tests at room and 316°C temperatures performed on the dry, thermo-cycled and thermo-cycled with moisture added M40J/PMR-II-50 and M60J/PMR-II-50 composites.

	M40J/PMR-II-50			M60J/PMR-II-50		
	Dry [MPa]	Dry and thermo-cycled [MPa]	Thermo-cycled and moisture [MPa]	Dry [MPa]	Dry and thermo-cycled [MPa]	Thermo-cycled and moisture [MPa]
At RT	30.3 ± 3.1	37.5 ± 3.6	57.6 ± 7.2	9.9 ± 2.5	16.7 ± 2.4	31.8 ± 3.3
At 316°C	56.5 (**54.9± 4.3)	(***61.7 ± 0.7)	47.1 ± 2.8	(***40.0 ± 5.8)	39.0 ± 3.5	24.9 ± 11.0

Number of * are the number of tests with onset of AE after the maximum load.

Table 7b. Shear stresses at the maximum loads from the Iosipescu tests at room and 316°C temperatures performed on the dry, thermo-cycled and thermo-cycled with moisture added M40J/PMR-II-50 and M60J/PMR-II-50 composites.

	M40J/PMR-II-50			M60J/PMR-II-50		
	Dry [MPa]	Dry and thermo-cycled [MPa]	Thermo-cycled and moisture [MPa]	Dry [MPa]	Dry and thermo-cycled [MPa]	Thermo-cycled and moisture [MPa]
At RT	86.7 ± 2.7	87.1 ± 1.4	88.3 ± 0.4	63.8 ± 0.4	61.1 ± 1.3	58.7 ± 1.6
At 316°C	61.2 ± 4.1	64.5 ± 2.9	51.6 ± 3.0	50.2 ± 0.8	50.4±1.7	50.6 ± 3.2

Table 8. Ratios between the shear stresses at the significant onset of AE and the maximum shear stresses (in percent).

	T650-35 (as-supplied)	M40J (as-supplied)	M40J (thermo-cycled)	M40J (thermo-cycled with moisture)	M60J (as-supplied)	M60J (thermo-cycled)	M60J (thermo-cycled with moisture)
RT	89.6%	34.9%	43.0%	65.0%	15.5%	27.3%	54.2%
316°C	83.4%	92.3% (**89.7%)	(***95.6%)	91.2%	(***79.7%)	77.3%	49.2%

Number of * are the number of tests with onset of AE after the maximum load.

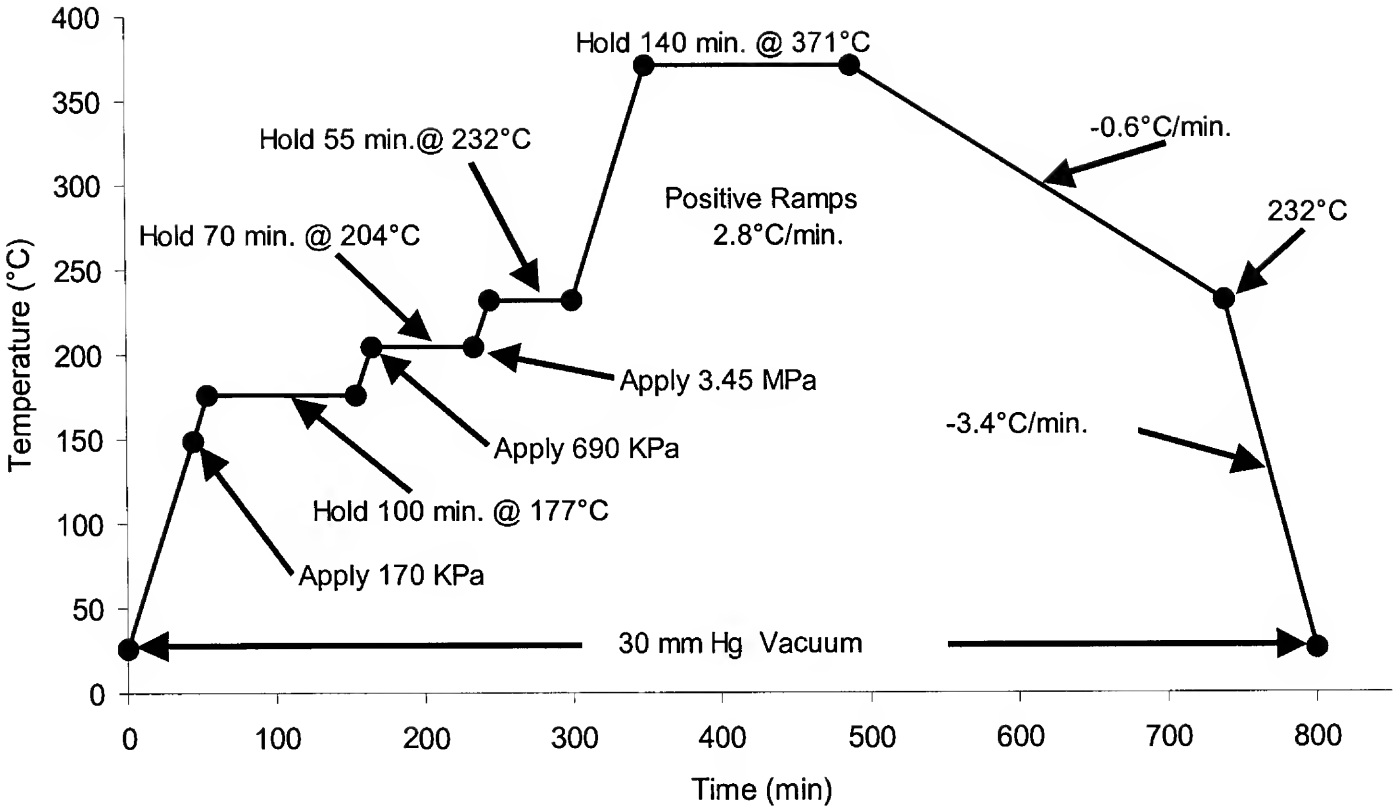

Figure 1a: Manufacturing cycle for the 4HS M40J/M60J/PMR-II-50 composite system.

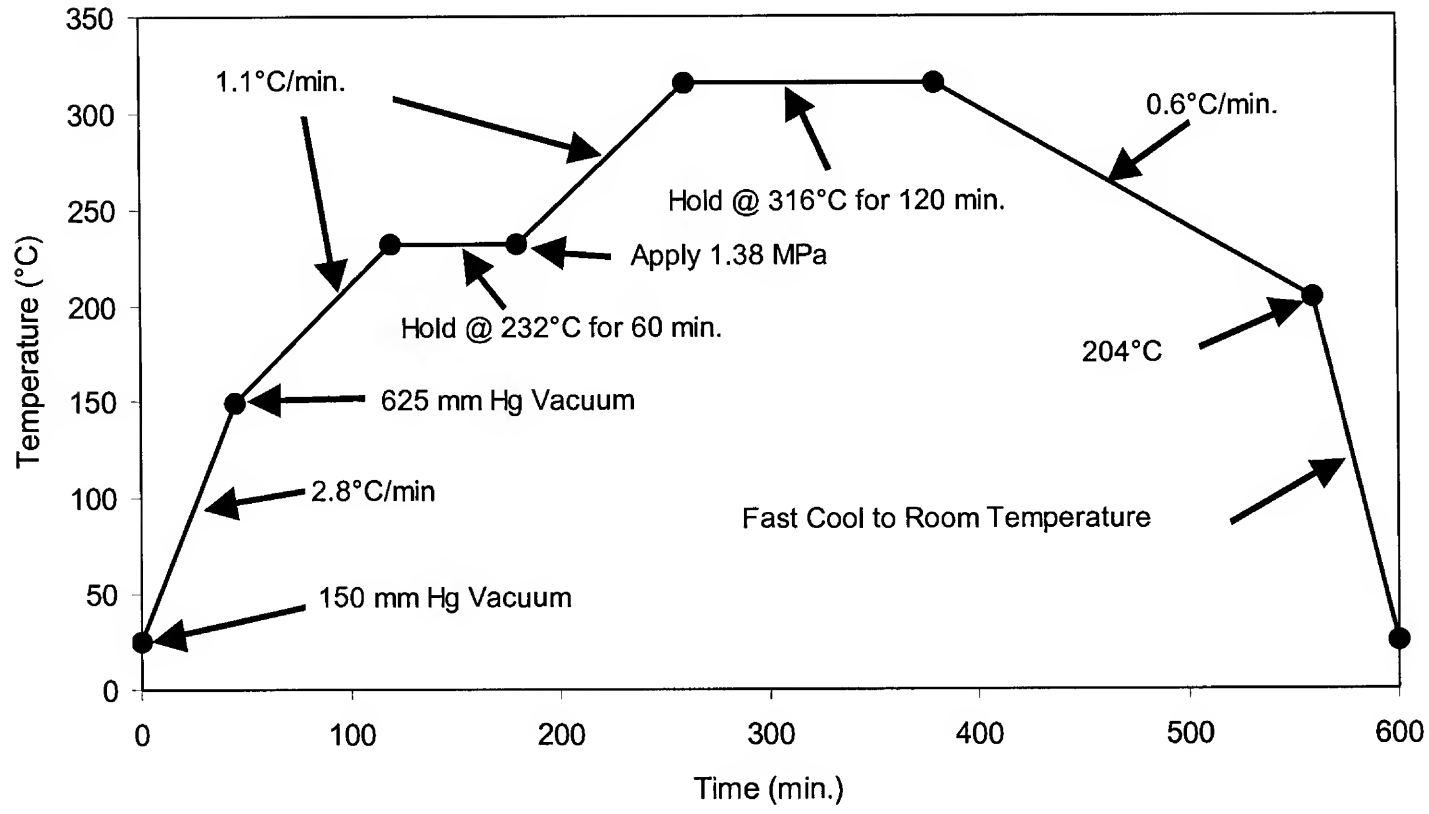

Figure 1b: Manufacturing cycle for the 8HS T-650/PMR-15 composite system.

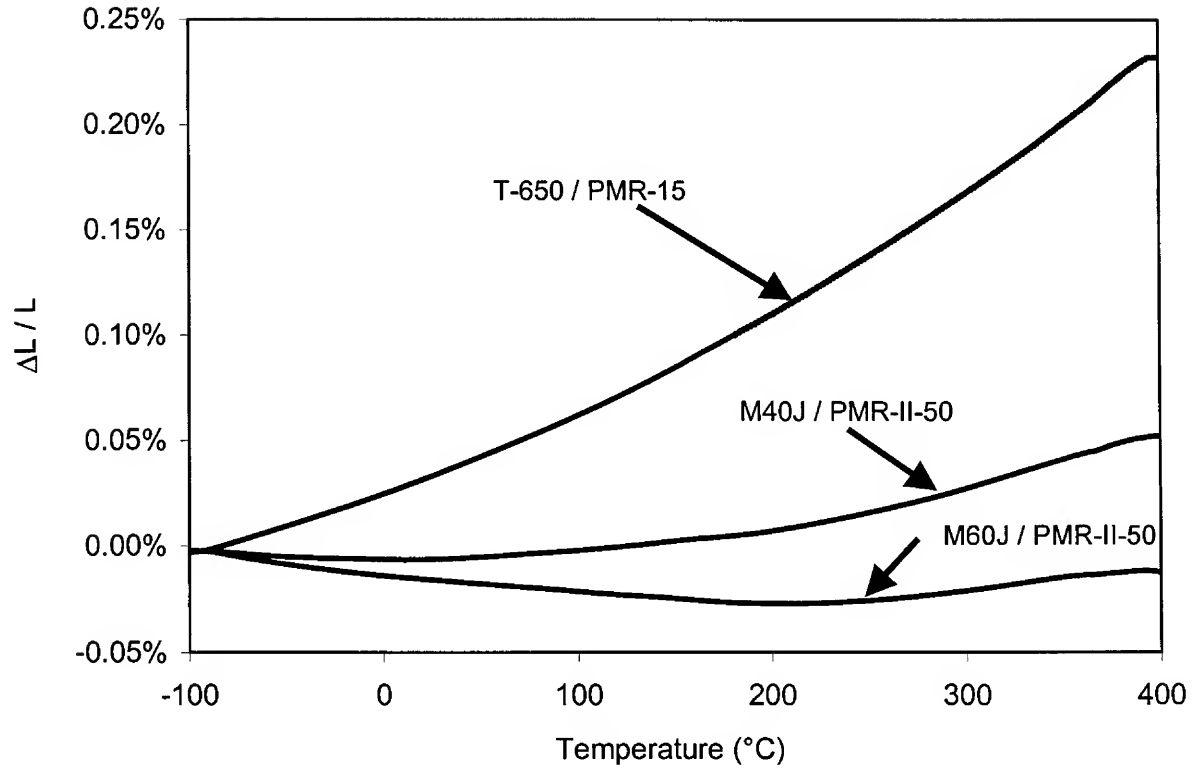

Figure 2a: Thermal expansions in-plane for the T-650/PMR-15, M40J/PMR-II-50 and M60J/PMR-II-50 composites as a function of temperature.

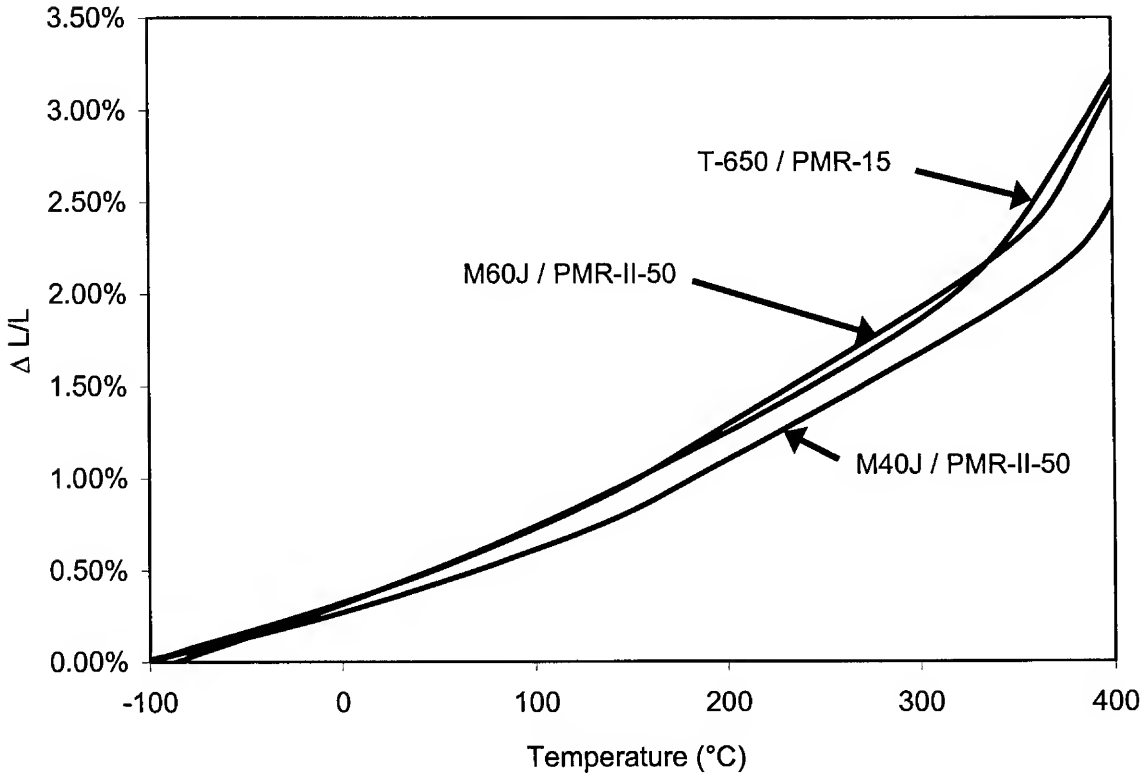

Figure 2b: Thermal expansions out-of-plane for the T-650/PMR-15, M40J/PMR-II-50 and M60J/PMR-II-50 composites as a function of temperature.

Figure 3: Optical micrograph of an as supplied 8HS T-650/PMR-15 composite.

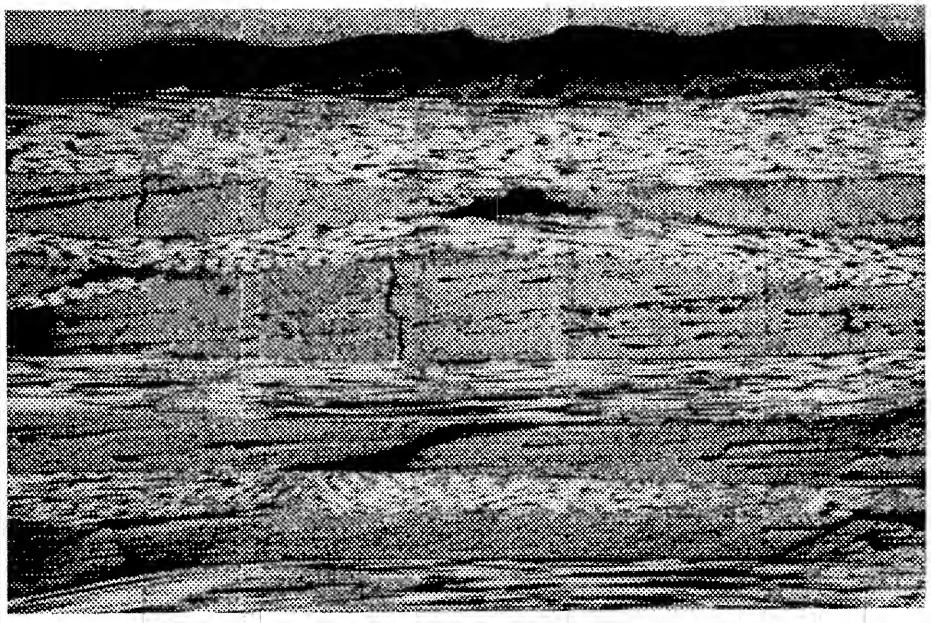

Figure 4a: Optical micrograph of as-supplied M40J/PMR-II-50.

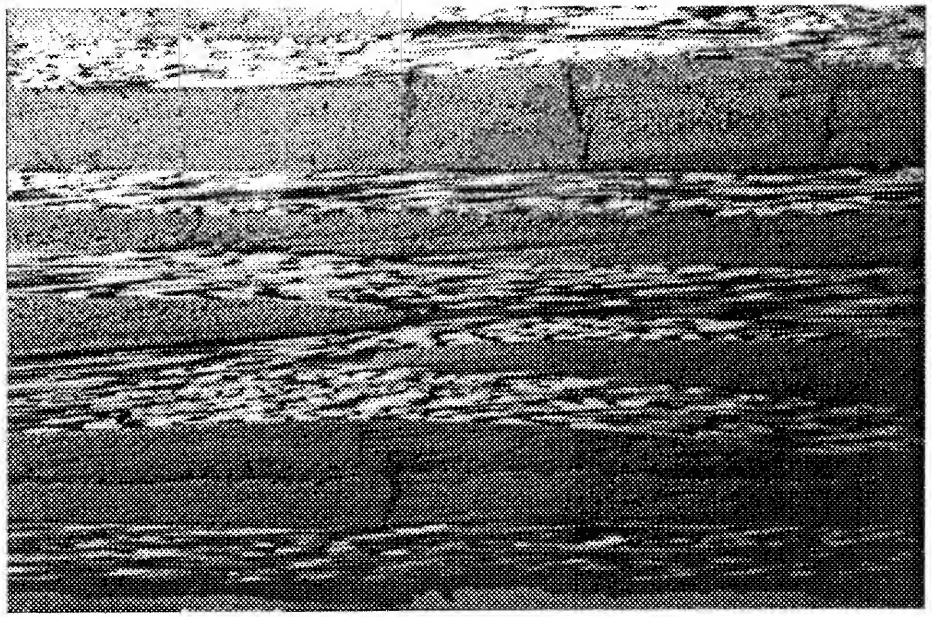

Figure 4b: Optical micrograph of thermo-conditioned M40J/PMR-II-50.

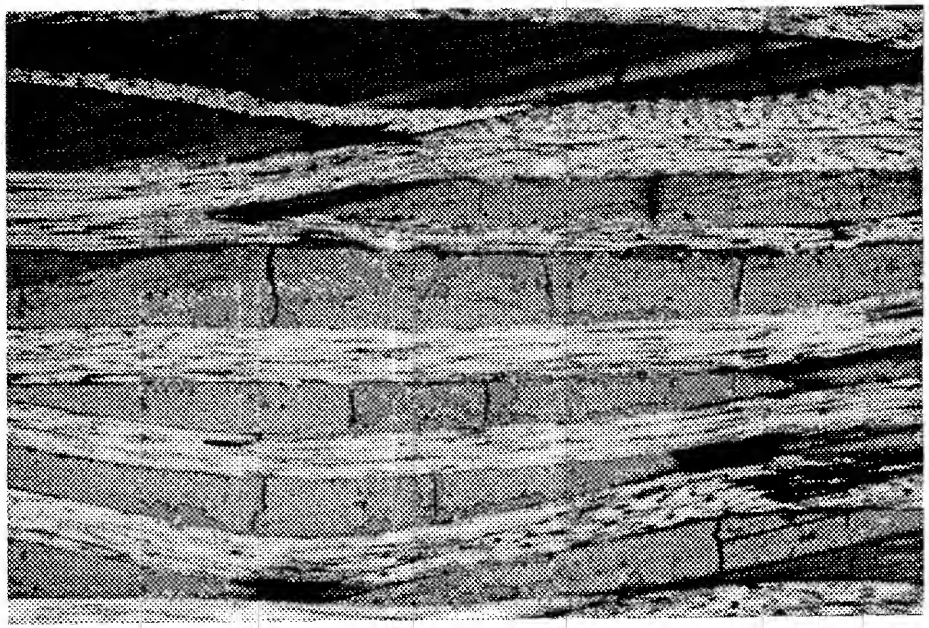

Figure 5a: Optical micrograph of as-supplied M60J/PMR-II-50.

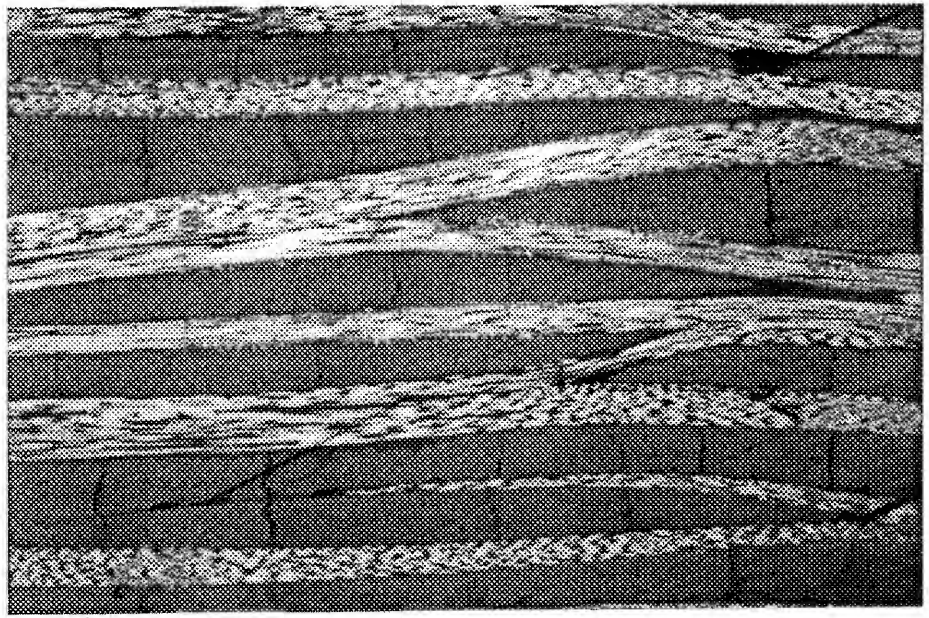

Figure 5b: Optical micrograph of thermo-conditioned M60J/PMR-II-50.

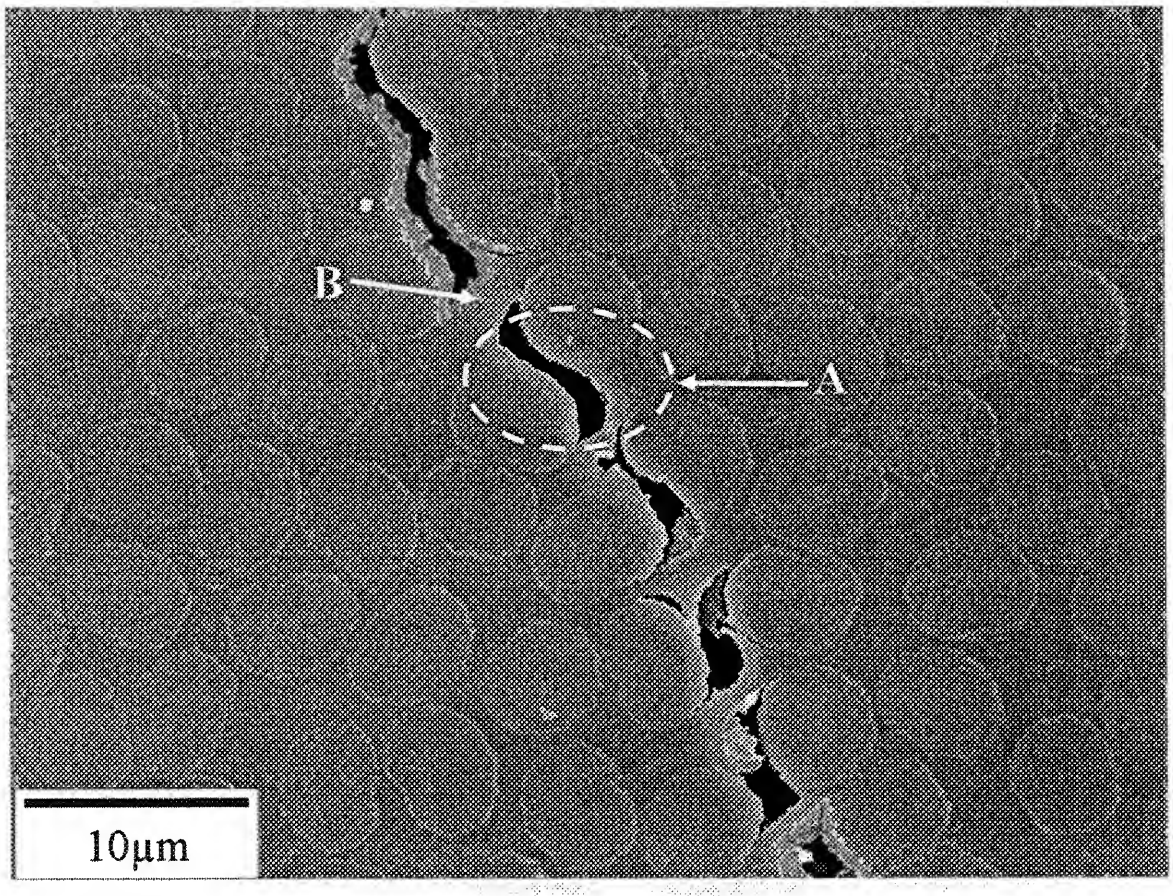

Figure 6a: SEM micrograph of as-supplied M40J/PMR-II-50.

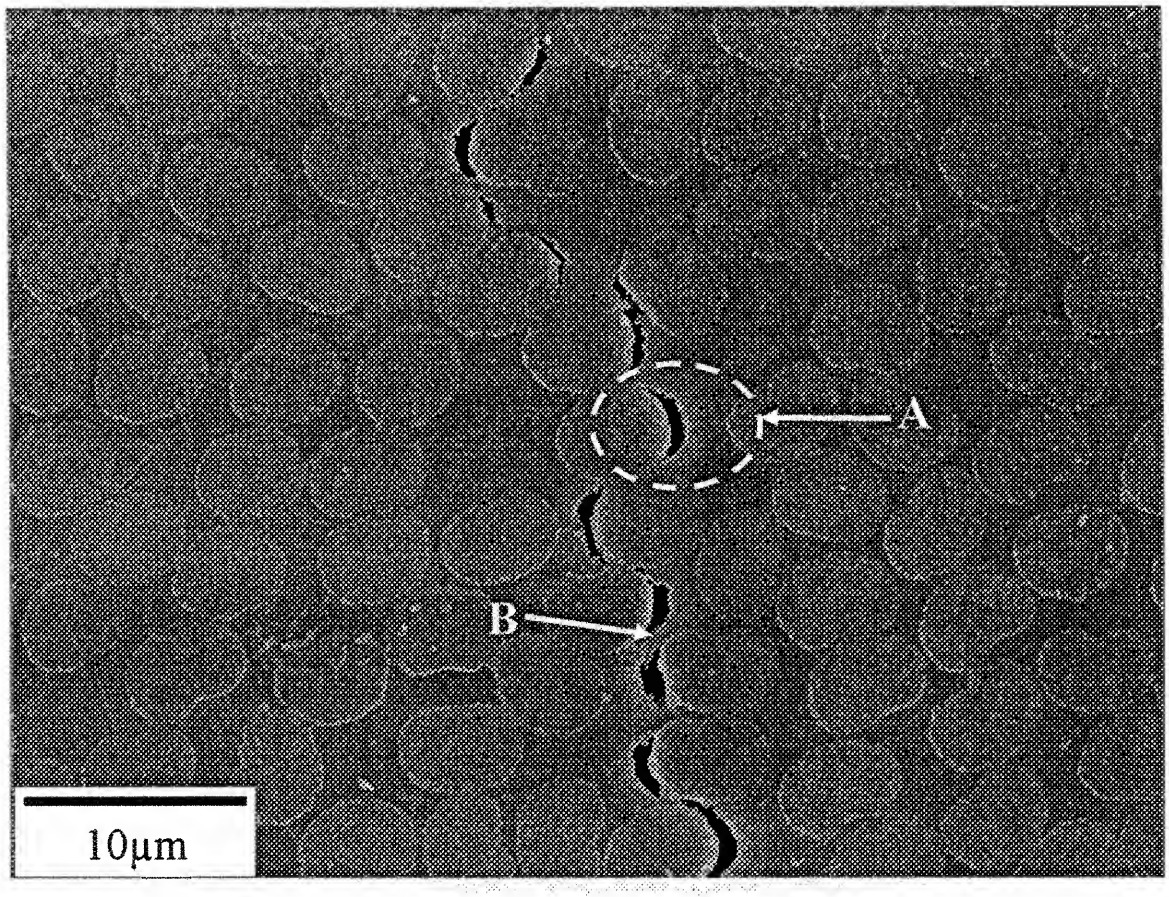

Figure 6b: SEM micrograph of as-supplied M60J/PMR-II-50.

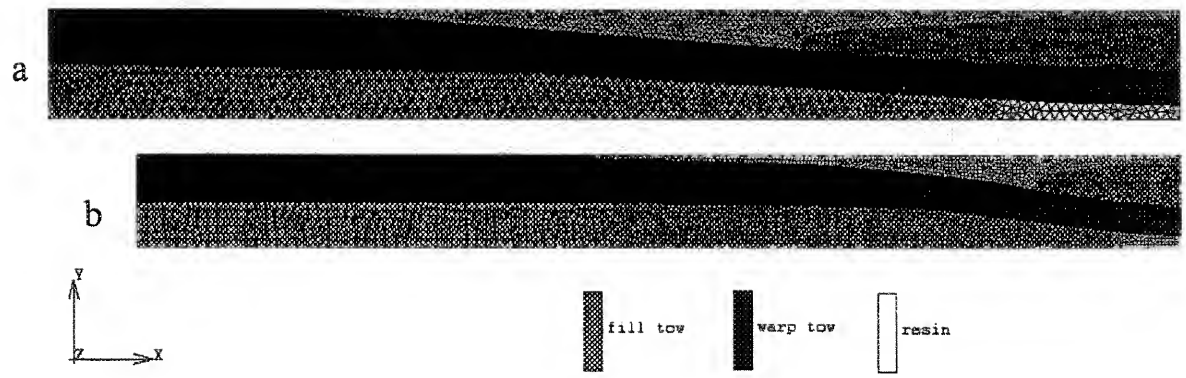

Figure 7: Two-dimensional finite element representations of the 4HS (a) and 8HS (b) composite architectures.

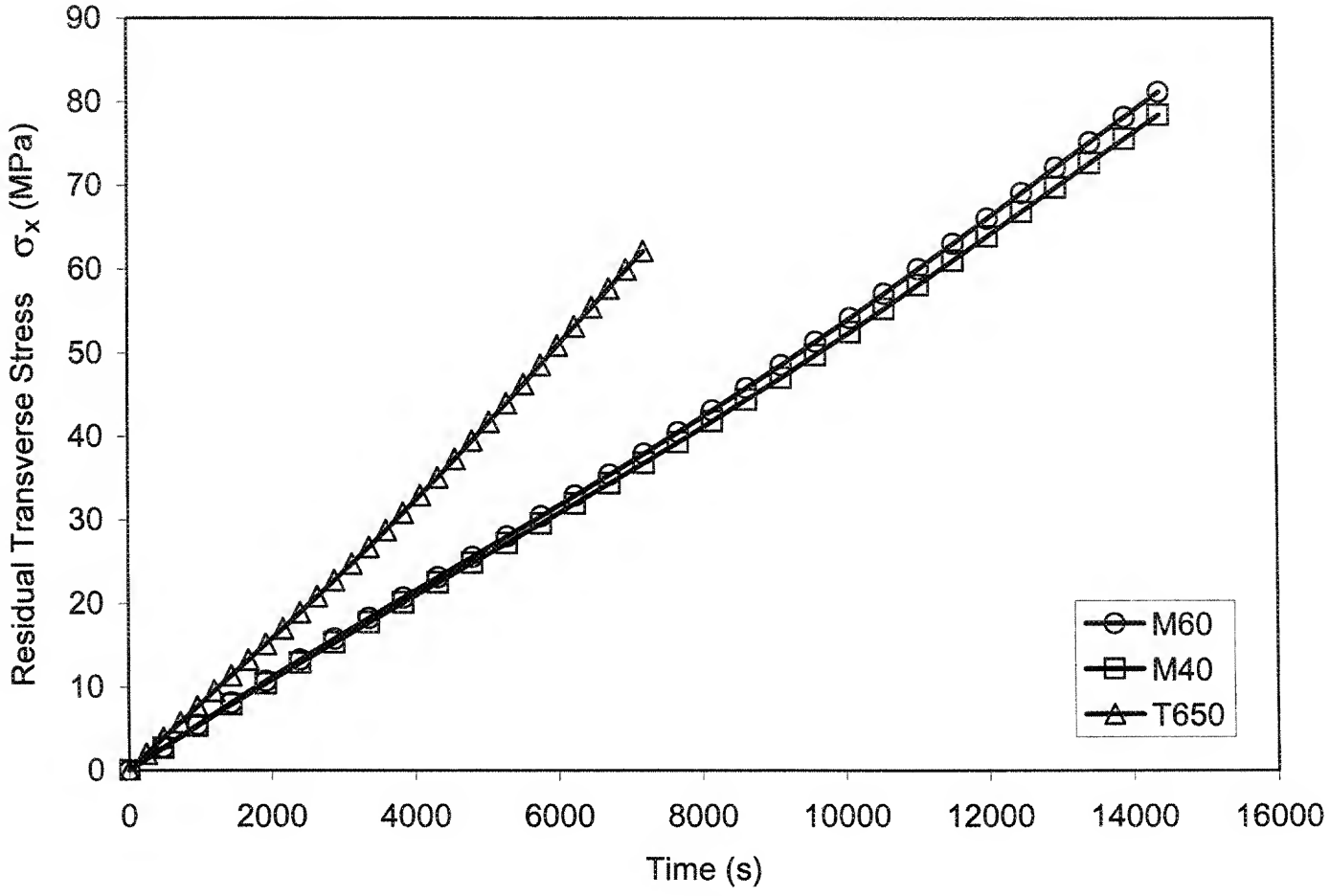

Figure 8: Residual transverse stresses σ_x in the middle of the fill tows as a function of time in the 8HS T-650/PMR-15, 4HS M40J/PMR-II-50 and M60J/PMR-II-50 composites. Starting time, t(0), is immediately following the high temperature 16hr. postcure isothermal.

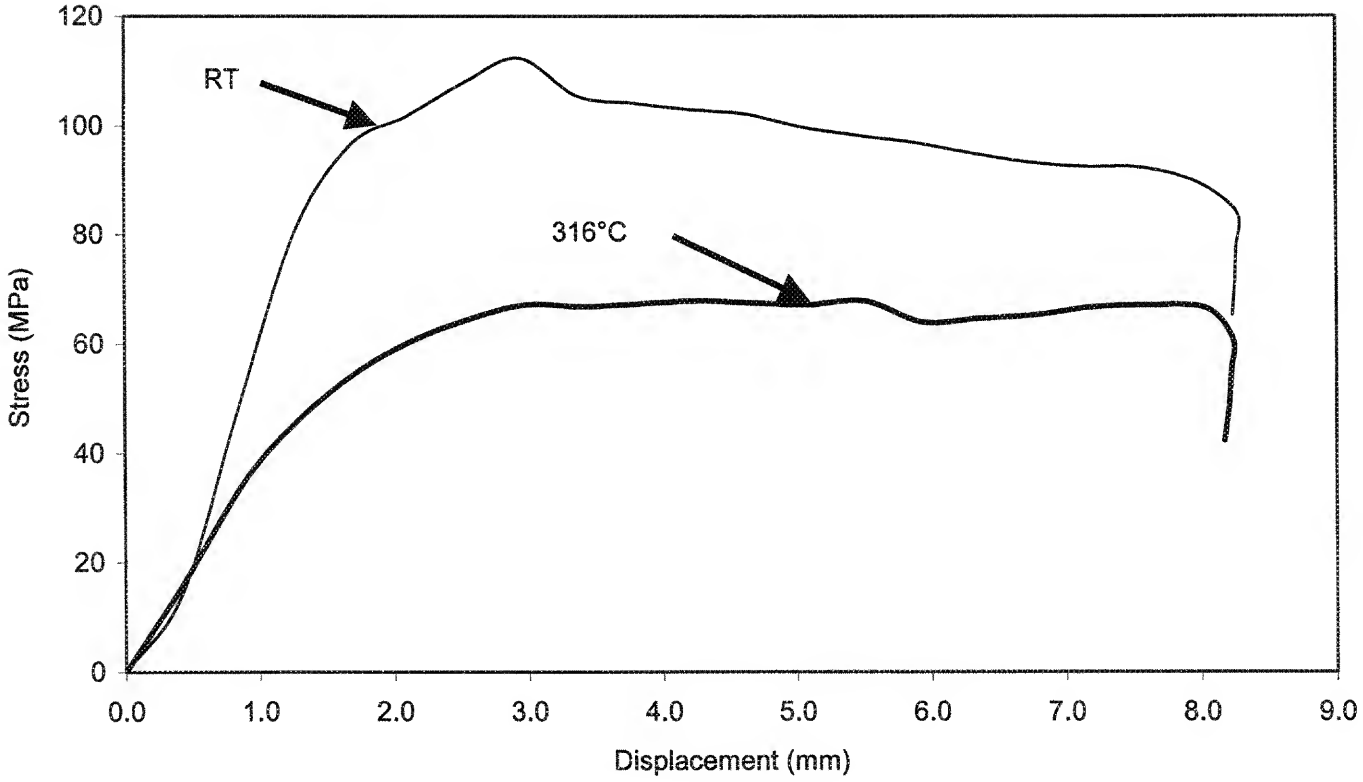

Figure 9: Typical stress vs. displacement diagrams for the T-650/PMR-15 tested at room and 316°C temperatures.

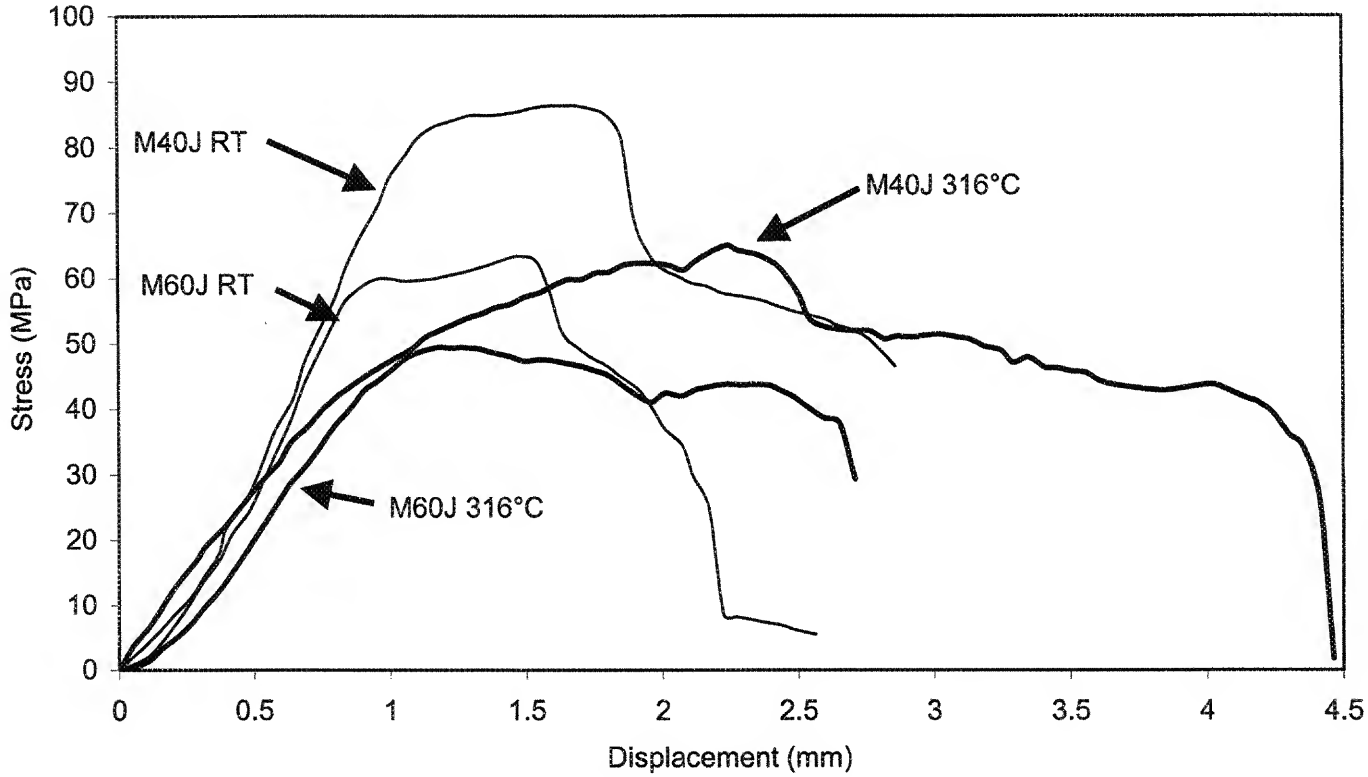

Figure 10: Typical stress vs. displacement diagrams for the M40J/PMR-II-50 and M60J/PMR-II-50 composites (all dry without thermo-cycling) tested at room and 316°C temperatures.

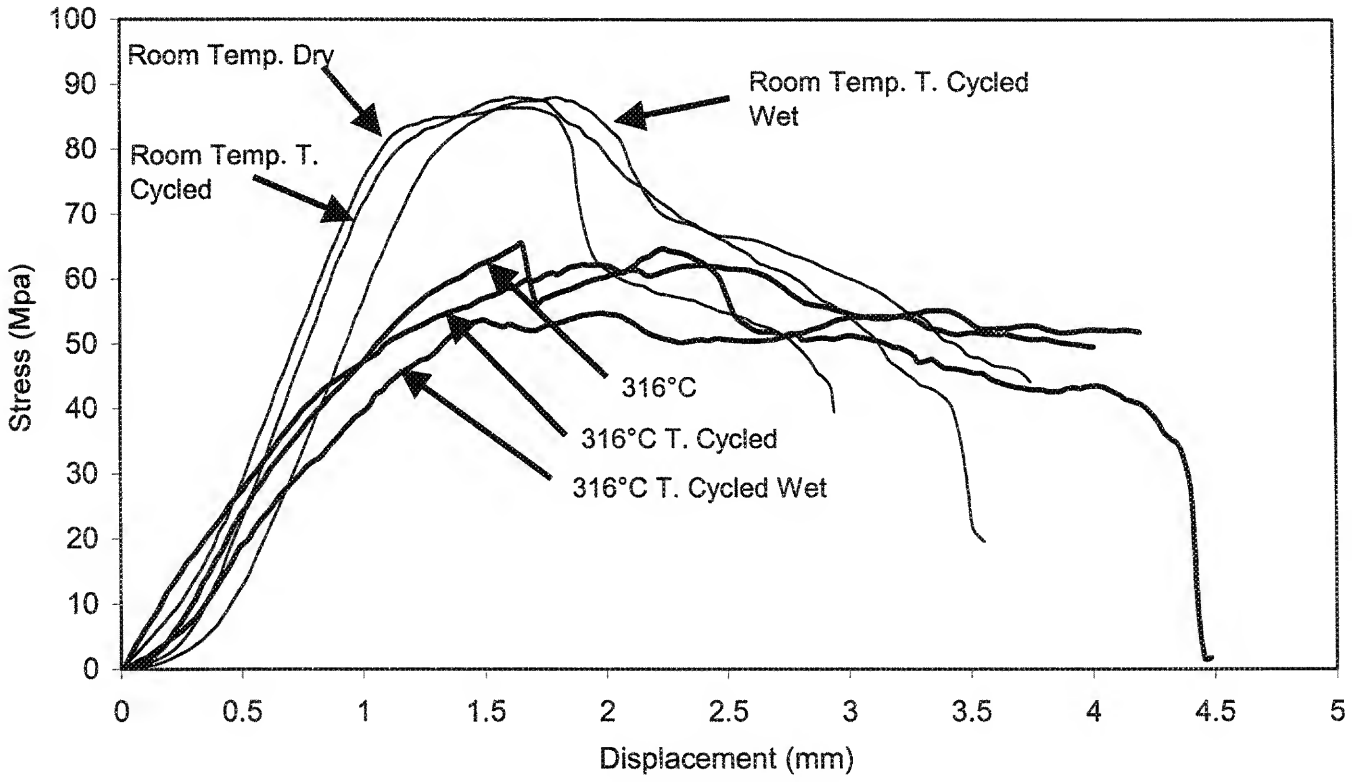

Figure 11a: Typical stress vs. displacement curves for the M40J/PMR-II-50 composites tested at room and at 316°C under dry, thermo-cycled and thermo-cycled with moisture conditions.

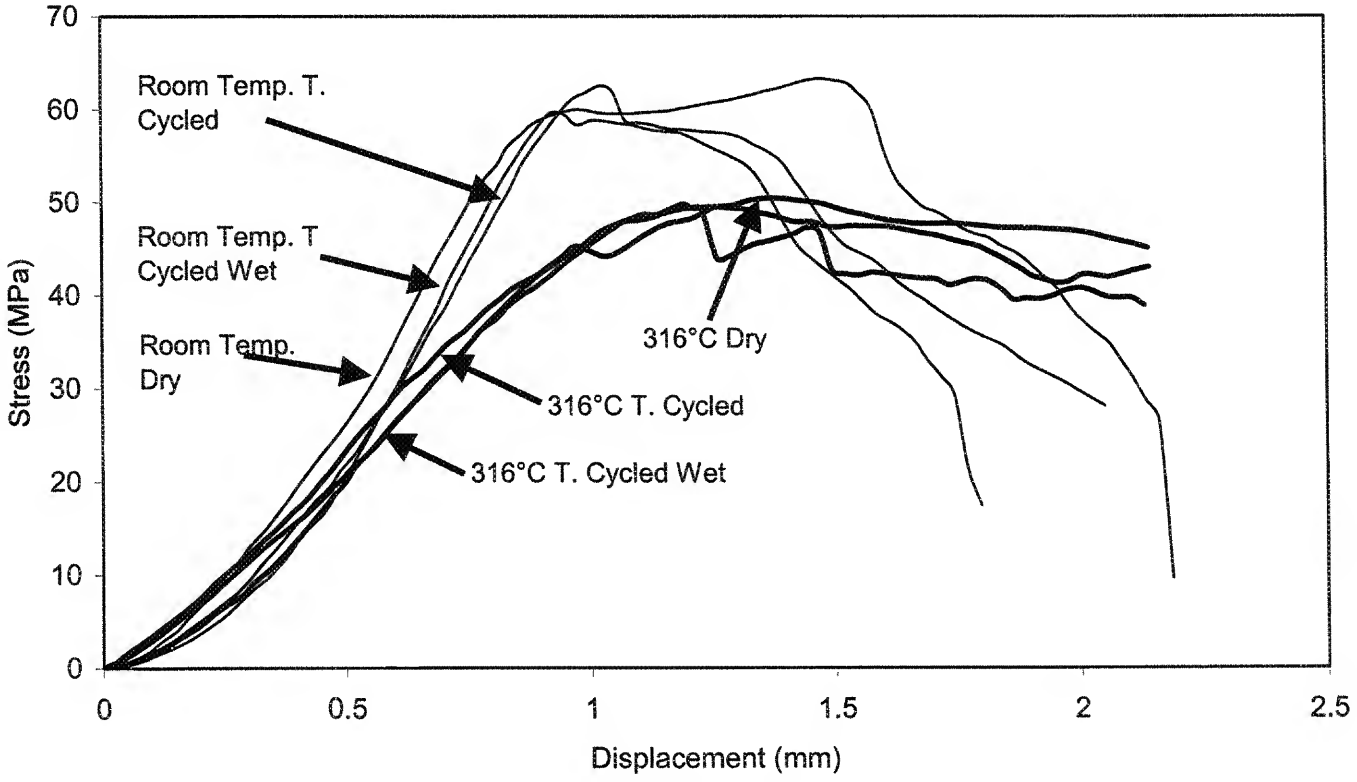

Figure 11b: Typical stress vs. displacement curves for the M60J/PMR-II-50 composites tested at room and at 316°C under dry, thermo-cycled and thermo-cycled with moisture conditions.

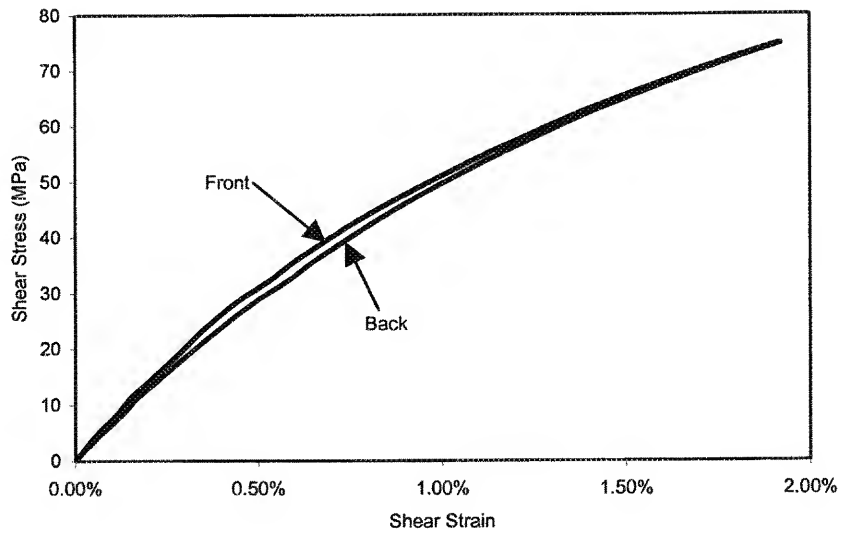

Figure 12a: Examples of stress strain curves from the front and back strain gages for the T-650/PMR-15 composites (as supplied) tested at room temperature.

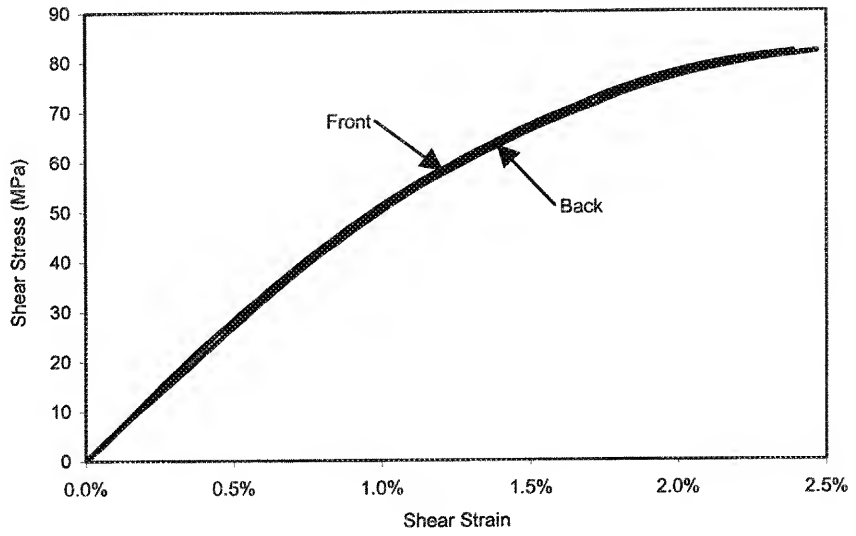

Figure 12b: Examples of stress strain curves from the front and back strain gages for the M40J/PMR-II-50 composites (as supplied) tested at room temperature.

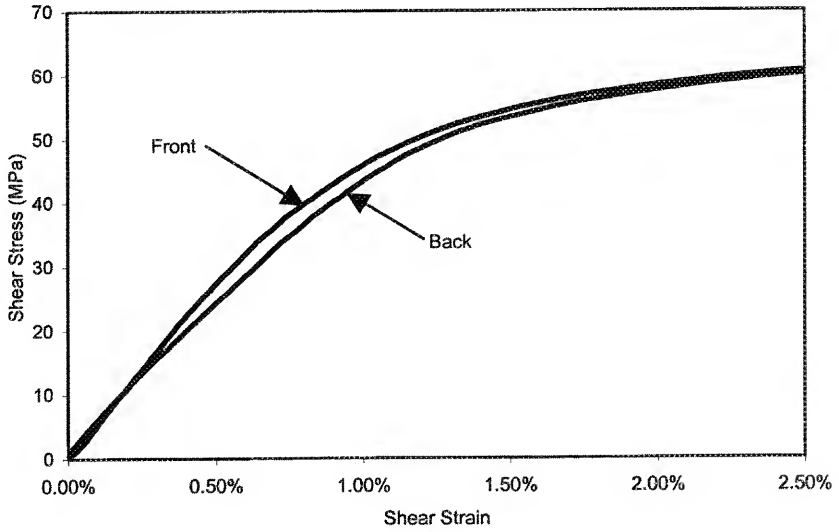

Figure 12c: Examples of stress strain curves from the front and back strain gages for the M60J/PMR-II-50 composites (as supplied) tested at room temperature.

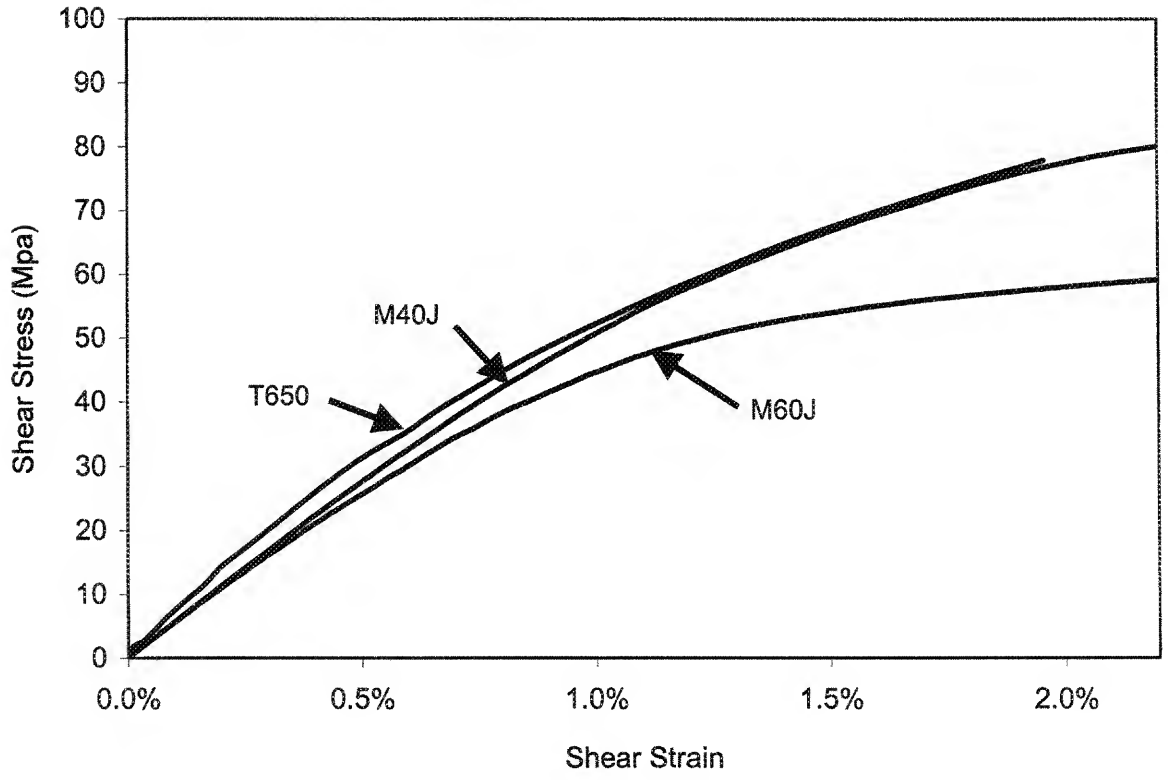

Figure 13: Shear stress vs. shear strain curves for the T-650/PMR-15, M40J/PMR-II-50 and M60J/PMR-II-50 composites (as supplied) tested at room temperature.

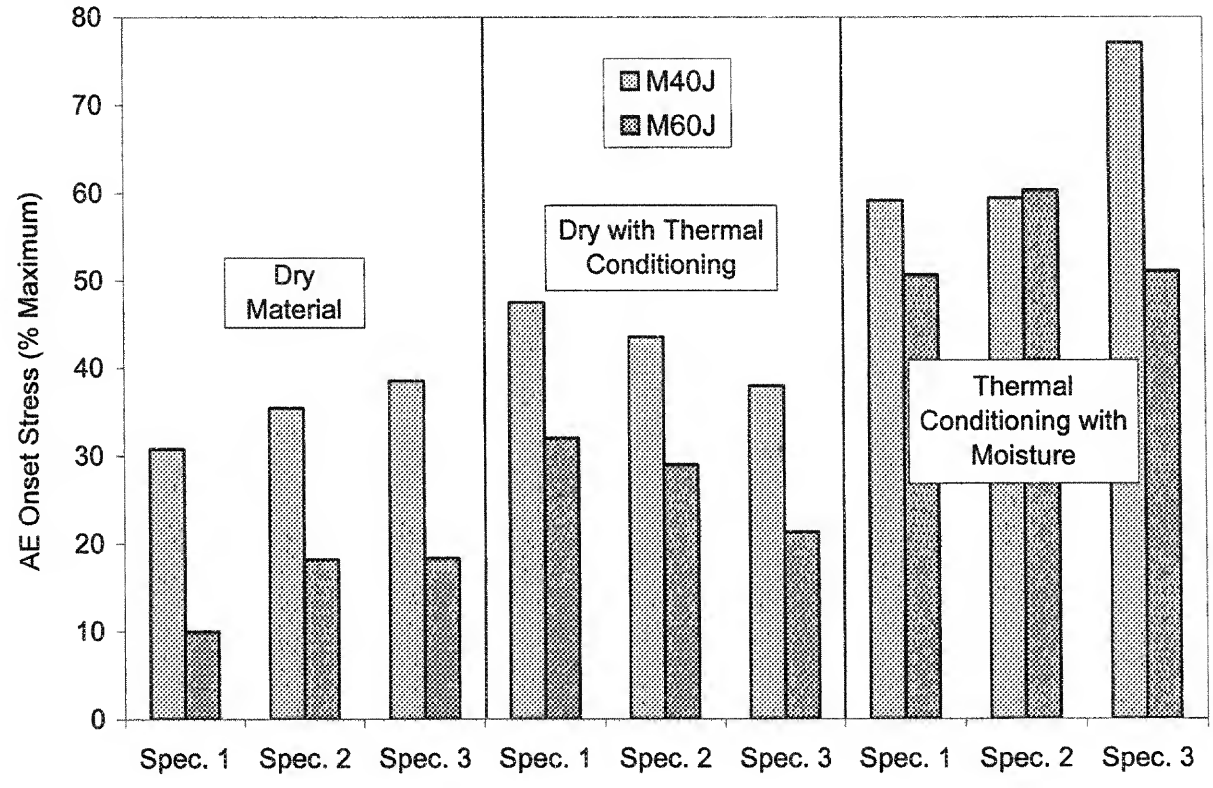

Figure 14: AE initiation stresses (% of the maximum stresses) for all the M40J/PMR-II-50 and M60J/PMR-II-50 specimens tested at room temperature.

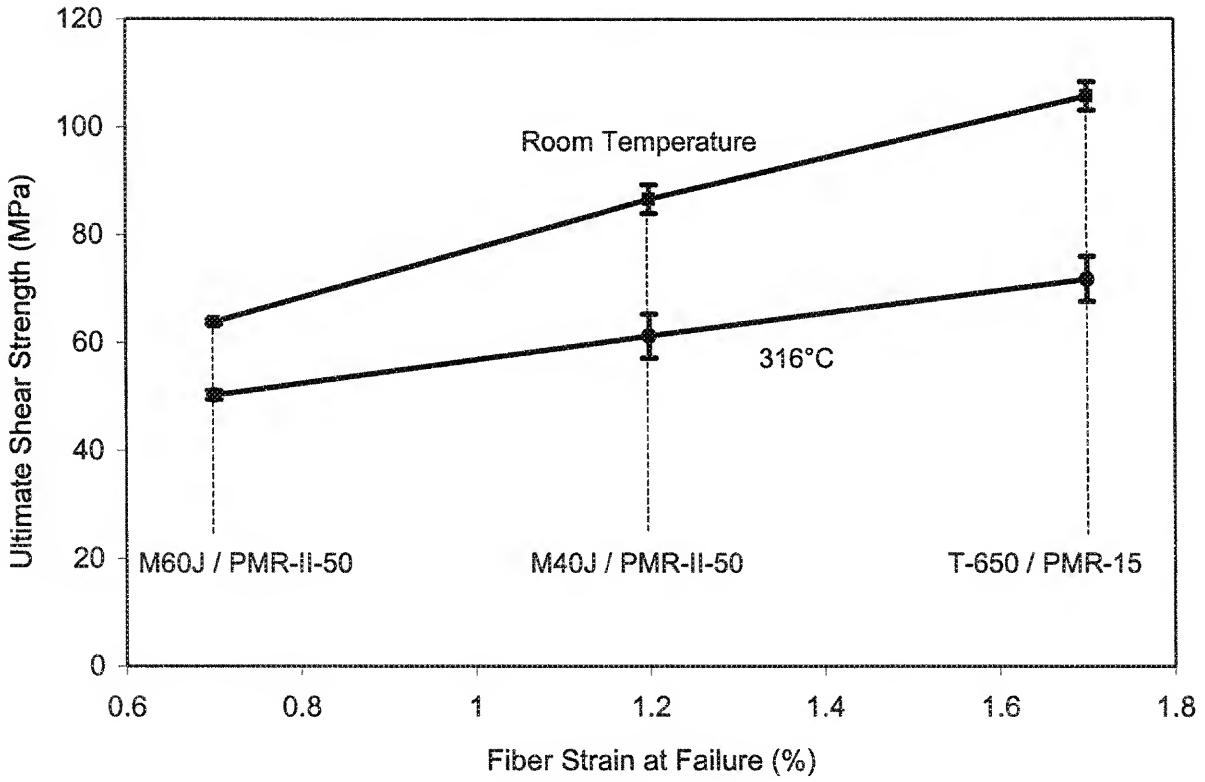

Figure 15: Shear strength of the as supplied T-650, M40J and M60J fiber composites at room temperature and 316°C as a function of the fiber strain at failure.